Surface Modification of Bone Implanted Materials by Layer-by-Layer Self Assembly Technique

Safitree Nawae

A Thesis Submitted in Fulfillment of the Requirements for the

Degree of Doctor of Philosophy in Physics

Prince of Songkla University

2019

Copyright of Prince of Songkla University

Surface Modification of Bone Implanted Materials by Layer-by-Layer Self Assembly Technique

Safitree Nawae

A Thesis Submitted in Fulfillment of the Requirements for the

Degree of Doctor of Philosophy in Physics

Prince of Songkla University

2019

Copyright of Prince of Songkla University

Thesis Title Surface Modification of Bone Implanted Materials by Layer-by-Layer Self Assembly Technique

Author Miss Safitree Nawae

Major Program Physics

Major Advisor

……..……..……
(Assoc. Prof. Dr.Nantakan Muensit)

Co-advisor

……..…..…..
(Asst. Prof. Dr.Chalongrat Daengngam)

Examining Committee:

…..……...……..……Chairperson
(Assoc. Prof. Dr.Wattanapong Kurdthongmee)

……...……...…..……..……Committee
(Assoc. Prof. Dr.Nantakan Muensit)

…..……..……...……...……..……Committee
(Asst. Prof. Dr.Chalongrat Daengngam)

……..……..…..……Committee
(Asst. Prof. Dr.Pornsuda Bomlai)

The Graduate School, Prince of Songkla University, has approved this thesis as fulfillment of the requirements for the Doctor of Philosophy Degree in Physics.

..……..……..……
(Prof. Dr.Damrongsak Faroongsarng)
Dean of Graduate School

This is to certify that the work here submitted is the result of the candidate's own investigations. Due acknowledgement has been made of any assistance received.

.....Signature
(Assoc. Prof. Dr.Nantakan Muensit)
Major Advisor

.....Signature
(Asst. Prof. Dr.Chalongrat Daengngam)
Co-advisor

.....Signature
(Miss Safitree Nawae)
Candidate

I hereby certify that this work has not been accepted in substance for any degree, and is not being currently submitted in candidature for any degree.

.....Signature
(Miss Safitree Nawae)
Candidate

ชื่อวิทยานิพนธ์ การดัดแปรพื้นผิวของวัสดุฝังทดแทนกระดูกด้วยเทคนิคการจัดเรียงตัวเองแบบทีละชั้น
ผู้เขียน นางสาวสาฟีตรี นาแว
สาขา ฟิสิกส์
ปีการศึกษา 2561

บทคัดย่อ

การดัดแปรพื้นผิวของรากฟันเทียมถูกนำมาใช้งานอย่างแพร่หลายในปัจจุบัน เพื่อเพิ่มการเกิดกระดูกเชื่อมประสาน และเกิดการสร้างกระดูกขึ้นมาใหม่รอบ ๆ รากฟันเทียม การศึกษาครั้งนี้สร้างฟิล์มบางโดยเทคนิคการจัดเรียงตัวเองแบบทีละชั้น ซึ่งสามารถควบควบคุมลำดับการจัดเรียงตัวขององค์ประกอบทางเคมีที่มีความแม่นยำสูงในการสร้างโครงสร้างระดับนาโน สารชีวโมเลกุลที่ใช้เป็นองค์ประกอบหลักคือ โปรตีนไหม (SF) และคอลลาเจนประเภทที่ 1 (Col) และใช้พอลิเมอร์ พอลิ(ไดอัลลิลไดเมทิลแอมโมเนียม คลอไรด์) (PDDA) เป็นตัวประสานเนื่องจากมีความเข้ากันได้ทางชีวภาพ ประกอบขึ้นเป็นฟิล์มบาง $[PDDA/SF/PDDA/Col]_n$ เมื่อ n คือจำนวนรอบของการสังเคราะห์ ขั้นตอนการสังเคราะห์ฟิล์มอาศัยแรงทางประจุไฟฟ้าระหว่างอนุภาค ซึ่งทั้งหมดนี้สามารถทำซ้ำเพื่อให้ได้ฟิล์มหลายชั้นที่มีความหนาตามต้องการ ตัวตรวจวัดการเปลี่ยนแปลงทางมวลถูกนำมาใช้ในการวิเคราะห์การก่อตัวของชั้นฟิล์มโดยควอตส์คริสตัลไมโครบาลานส์ โครงสร้างจุลภาคของฟิล์มบางวิเคราะห์โดยกล้องจุลทรรศน์อิเล็กตรอนแบบส่องกราดและกล้องจุลทรรศน์แรงอะตอม และศึกษาลักษณะความชอบน้ำของพื้นผิวฟิล์มด้วยเทคนิควัดมุมสัมผัสของของเหลว วิเคราะห์การจัดโครงสร้างของพื้นผิวฟิล์มโดยใช้หลักการดูดกลืนรังสีอินฟาเรดด้วยเทคนิคฟูเรียร์ทรานส์ฟอร์มอินฟราเรดสเปคโตรสโคปและเทคนิครามานสเปคโตรสโคป งานวิจัยนี้ได้ตรวจสอบความเข้ากันได้ทางชีวภาพของฟิล์มบางกับเซลล์สร้างกระดูกออสติโอบลาสต์ โดยประเมินประสิทธิภาพการตอบสนองของเซลล์กระดูกจากการทดสอบการกระตุ้นการแบ่งเซลล์ อีกทั้งศึกษาความสามารถการเปลี่ยนแปลงของเซลล์ต้นกำเนิดจากเยื่อหุ้มกระดูกไปเป็นเซลล์กระดูกด้วยวิธีตรวจค่าแอลคาไลน์ฟอสฟาเทส จากการศึกษาพบว่าความหนาฟิล์มบางที่เตรียมได้เพิ่มขึ้นตามจำนวนรอบของการสังเคราะห์ทุก 7 นาโนเมตร และสัมพันธ์กับค่าความขรุขระพื้นผิวเฉลี่ยที่เพิ่มขึ้นซึ่งส่งผลดีต่อการยึดเกาะของเซลล์ สเปกตรัมการดูดกลืนคลื่นแสงของหมู่ฟังก์ชันของฟิล์มบางที่เตรียมได้พบว่า การสั่นของหมู่ฟังก์ชันเอไมด์ I เอไมด์ II และเอไมด์ III แสดงอย่างชัดเจน ทั้งหมดนี้แสดงถึงลักษณะของฟิล์มบางที่มีความหยาบ

มีความชอบน้ำ และมีการตอบสนองของเซลล์ที่ดี ผลการศึกษาเบื้องต้นพบว่าจำนวนรอบการสังเคราะห์ฟิล์มที่ 40 และ 50 มีความเหมาะสมต่อการตอบสนองของเซลล์กระดูก จากการศึกษาแสดงให้เห็นถึงฟิล์มบางที่เตรียมได้โดยวิธีจัดเรียงตัวเองแบบทีละชั้นมีแนวโน้มสามารถเพิ่มการเกิดกระดูกเชื่อมประสาน ผลที่ได้นี้เป็นแนวทางที่สำคัญในการพัฒนาวิธีการนำไปประยุกต์ใช้งานทางคลินิกต่อไป

Thesis title Surface Modification of Bone Implanted Materials by Layer-by-Layer Self Assembly Technique
Author Miss Safitree Nawae
Major Program Physics
Academic Year 2018

ABSTRACT

In recent years, surface modifications for dental implants have evolved rapidly, particularly for enhanced osseointegration and bone formation around implants. In this study, a powerful layer-by-layer self-assembly (LbL) technique was employed to fabricate thin film through precise control of the chemical composition and film morphology on a nanoscale level. Potent biomaterials were used for the multilayer coating, including silk fibroin (SF), type I collagen (Col), and poly(diallydimethylammonium chloride) (PDDA), which each impart the surface with a combination of biomechanical, physiochemical, and hydrophilic wetting properties. These materials were assembled sequentially via electrostatic interaction in an aqueous solution phase to produce a $[PDDA/SF/PDDA/Col]_n$ thin film with different n quad-layers: $n = 0$ (control), 10, 20, 30, 40, and 50. The multilayer formation, topography, morphology, and the surface characteristics of the films were tested and analyzed using quartz crystal microbalance, atomic force microscopy, scanning electron microscopy, and wettability, respectively. The molecular organization of the films was characterized by Fourier transform infrared and Raman spectroscopy. Meanwhile, their biological performance was evaluated using osteoblast cell proliferation, alkaline phosphatase (ALP) activity, and total protein absorption. The thickness of multilayer film can be changed by increasing the number of quad-layers adsorbed with an increment of 7 nm. It was also found that the surface topography was affected by the number of quad-layers as the root mean square roughness of the film increased as a function of n in a range of tens of nanometers, which is beneficial for initial cell adhesion. The multilayer films demonstrated the mobility of amide I, II, III, and molecular skeletal vibration. The films exhibited rough surfaces, hydrophilicity, and were able to enhance cell proliferation, ALP activity, and total protein absorption. Preliminary results appear the optimum of

the number of quad-layers between 40 and 50. The results indicate that self-assembled LbL films are promising for use as a nucleating surface for osseointegration in the design of coated dental implant materials and could serve as the foundation for further clinical applications.

ACKNOWLEDGEMENTS

"In the name of Allah, the Most Gracious and the Most Merciful"

Alhamdulillah, I praise and thank Allah for His greatness and for giving me the strength and courage to complete this thesis. The completion of this thesis would be quite impossible without the help of many people and sources of funding. I wish to express my gratitude to those that have contributed to the completion of this thesis:

First and foremost, I would like to express my deepest thanks to my advisor, Associate Professor Dr. Nantakan Muensit, for her suggestion, encouragement and supervision throughout my graduate studies. Her instructions and complete support conducted my working and learning experience. I would also like to express my gratitude to my co-advisor, Assistant Professor Dr. Chalongrat Daengngam, for his valuable guidance, suggestion and encouragement. I appreciate all his contributions of time, support and ideas. Not forgotten, my appreciation to Associate Professor Dr. Jirut Meesane, for his support and invaluable help of constructive comments throughout the experimental.

I highly thank the Examining Committee, Associate Professor Dr. Wattanapong Kurdthongmee, School of Engineering and Resources, Walailak University; and Assistant Professor Dr. Pornsuda Bomlai, Department of Materials Science and Technology, Prince of Songkla University, for taking time out of their busy schedules to evaluate my work.

I'd like to present my sincere thankfulness to Professor Dr. Feng-Huei Lin, Institute of Biomedical Engineering, National Taiwan University, for his support me to be a research visiting student under his supervision for 6 months.

Special thanks go to my dear father and my deceased mother, who suffered from brain tumor through 7 years and died peacefully in October 2017. I also thank my husband, Akabar Yakoh, for his love and endless care encouraged at every stage of my personal and academic life. Thank you, my cute little daughter, Nada Yakoh, for being a good kid which always make me happy in mind without fear during an education.

I would never forget all my friends in the Material Physics Laboratory and the other laboratories, for their grateful helping hand. Furthermore, I would like to thank everybody who was important to the successful realization of this thesis, as well as expressing my apology that I could not mention personally one by one.

Finally, I would like to acknowledge financial support from: the Office of the Higher Education Commission (OHEC) Thailand, under the Strategic Scholarships Fellowships Frontier Research Networks (Specific for Southern region), and the Prince of Songkla University (PSU) Graduate School. I also appreciate the support of Department of Physics, Faculty of Science, Prince of Songkla University; the Center of Excellence in Nanotechnology for Energy (CENE); the Biological Materials for Medicine (BMM) Research Unit, Institute of Biomedical Engineering, Faculty of Medicine, Prince of Songkla University; Princess of Naradhiwas University (PNU); and Queen Sirikit Sericulture Centre, Narathiwat, for providing me research equipment and all the things that facilitated smooth work of my research.

Safitree Nawae

TABLES OF CONTENTS

ABSTRACT (Thai) V
ABSTRACT (English) VII
ACKNOWLEDGEMENTS IX
TABLES OF CONTENTS XI
LIST OF FIGURES XIV
LIST OF TABLES XVI
LIST OF ABBREVIATIONS AND SYMBOLS XVII

CHAPTER 1: INTRODUCTION 1
1.1 Background and Motivation of the Research 1
1.2 Objectives of research 4
1.3 Thesis outline 4

CHAPTER 2: THEORETICAL BACKGROUND 5
2.1 Introduction to Tissue Engineering 5
2.1.1 Tissue engineering of bone 5
2.1.2 Collagen for tissue engineering 7
2.1.3 Silk fibroin for tissue engineering 10
2.2 Osseointegration of Dental Implants 13
2.3 Implant Surface Modifications on Osseointegration 14
2.3.1 Topography and roughness of implant surface 15
2.3.2 The surface wettability 16
2.3.3 Methods of surface modification of implant 16
2.4 Layer-by-Layer Self-Assembly 23
2.4.1 The basic principle of LbL technique 23
2.4.2 Methods operated in LbL Self-assembly 24
2.4.3 Advantages of LbL modified implant surface 25

TABLES OF CONTENTS (cont.)

CHAPTER 3: RESEARCH METHODOLOGY 26
3.1 Preparation of Aqueous Silk Fibroin Solution 26
3.2 Preparation of Type I Collagen 27
3.3 Preparation of PDDA Solution 28
3.4 Cleaning Processes Based on Hydrogen Peroxide 29
3.5 Multilayer Film Preparation 29
3.6 The Quartz Crystal Microbalance Measurement 30
3.7 Wettability and Surface Energy Measurement 32
3.8 Scanning Electron Microscopy 34
3.9 Atomic Force Microscopy 34
3.10 Fourier Transform Infrared Spectroscopy 34
3.11 Raman Spectroscopy 35
3.12 Cell Culture 35
3.13 Cell Proliferation 35
3.14 Alkaline Phosphatase Activity 36
3.15 Total Protein Assay 36
3.16 Nano-indentation Measurement 37
3.17 Statistical Analysis 39

CHAPTER 4: RESULTS AND DISCUSSION 40
4.1 Self-assembled Multilayer Formation 40
4.2 Topographical and Morphological Observation 41
4.3 Wetting Properties of the LbL Self-assembled Films 45
4.4 Fourier Transform Infrared Spectroscopy Characterization 48
4.5 Raman Spectroscopy 49
4.6 Cell Proliferation on LbL Self-assembled Films 51
4.7 Alkaline Phosphatase Activity on LbL Self-assembled Films 52
4.8 Total Protein on LbL Self-assembled Films 53

TABLES OF CONTENTS (cont.)

4.9 Mechanical Properties 55
4.10 Practical Use 57

CHAPTER 5: CONCLUSIONS AND FUTURES WORK 59
5.1 Conclusions 59
5.5 Future Works 59

REFERENCES 61
VITAE 73

LIST OF FIGURES

Figure 2.1	Structure of collagen triple helix.	8
Figure 2.2	Relative percentage on silk-based in vitro engineering of various tissues.	10
Figure 2.3	Schematic of the main components of *B. mori* cocoon.	11
Figure 2.4	The different stages of spin coating. (a) Dispensation, (b) Acceleration, (c) Flow dominated,(d) Evaporation dominated.	17
Figure 2.5	Scheme of the dip coating process.	18
Figure 2.6	Process of a plasma spray.	19
Figure 2.7	Versatility of LbL assembly. (a) Schematic overview of LbL assembly; (b) an overview showing that assembly technology influences film and process properties as well as application areas.	21
Figure 2.8	LbL assembly technologies. (a)-(e) Schematics of the five major technology categories for LbL assembly.	22
Figure 2.9	LbL self-assembly based on electrostatic interaction.	24
Figure 2.10	LbL coated titanium dental implant and localized delivery of substance to its surrounding environments to provide some benefit effects.	25
Figure 3.1	Schematic of the silk fibroin extraction procedure.	27
Figure 3.2	Schematic of the collagen extraction procedure.	28
Figure 3.3	Schematic of 1 quad PDDA/SF/PDDA/Col LbL self-assembly formation on a glass slide surface.	30
Figure 3.4	Schematic diagram of the QCM system.	31
Figure 3.5	Determination of polar and dispersive components of SFE.	33
Figure 3.6	Cantilever deflection.	37
Figure 3.7	The deflection curve of glass slide and polymer.	38
Figure 4.1	Frequency shift and stability for self-assembled layers of PDDA, SF, and Col.	41
Figure 4.2	Surface topology of $[PDDA/SF/PDDA/Col]_n$ film studied by AFM.	42

LIST OF FIGURES (cont.)

Figure 4.3	Surface roughness values of $[PDDA/SF/PDDA/Col]_n$ film determined from AFM analysis.	43
Figure 4.4	SEM images demonstrating the surface of $[PDDA/SF/PDDA/Col]_n$ film after LbL deposition.	44
Figure 4.5	Thickness of the self-assembled $[PDDA/SF/PDDA/Col]_n$ multilayer films evaluated by AFM.	44
Figure 4.6	Cross-sectional SEM image (50,000x) of $[PDDA/SF/PDDA/Col]_n$ film.	45
Figure 4.7	Water contact angle of $[PDDA/SF/PDDA/Col]_n$ film.	46
Figure 4.8	Representative SFE calculation graph based on the OWRK model for glass and multilayer film.	46
Figure 4.9	Surface free energy of $[PDDA/SF/PDDA/Col]_n$ film.	47
Figure 4.10	FTIR spectra of $[PDDA/SF/PDDA/Col]_n$ film.	49
Figure 4.11	Raman spectra of $[PDDA/SF/PDDA/Col]_n$ films.	50
Figure 4.12	WST-1 assay of MC3T3-E1 cells grown on $[PDDA/SF/PDDA/Col]_n$ film at days 1, 3, 5, and 7.	52
Figure 4.13	ALP activity of MC3T3-E1 cells cultured on $[PDDA/SF/PDDA/Col]_n$ film at days 7, 14, and 21.	53
Figure 4.14	Total protein content of MC3T3-E1 cells on $[PDDA/SF/PDDA/Col]_n$ film.	54
Figure 4.15	Typical mechanical curves obtained by AFM indentation.	55
Figure 4.16	A relationship between Young's modulus of $[PDDA/SF/PDDA/Col]_{50}$ film to ambient temperature arisen from 23 ^oC to 37 ^oC.	56
Figure 4.17	The change in Young's modulus of $[PDDA/SF/PDDA/Col]_{50}$ film.	57
Figure 4.18	Surface free energy and water contact angle of titanium surface.	58
Figure 4.19	The AFM surface topology image of titanium.	58
Figure 4.20	The surface morphological SEM image (50,000x) of $[PDDA/SF/PDDA/Col]_n$ film on titanium substrate.	58

LIST OF TABLES

Table 2.1	Advantages and disadvantages of collagen as biomaterial.	8
Table 2.2	The various collagen types as they belong to the major collagen families.	9
Table 2.3	Comparison of mechanical properties of natural silks and other materials.	12
Table 2.4	Advantages and disadvantages of silk as biomaterial.	13
Table 2.5	Advantages and disadvantages for methods operated in LbL self-assembly.	24
Table 3.1	Surface tension (SFT) of the test liquids.	32

LIST OF ABBREVIATIONS AND SYMBOLS

a	=	contact radius
AFM	=	atomic force microscopy
Ala	=	alanine
ALP	=	alkaline phosphatase
ATR	=	attenuated total reflection
BCA	=	bicinchoninic acid
BMPs	=	bone morphogenetic proteins
B. mori	=	*Bombyx mori*
CA	=	contact angle
Col	=	type I collagen
D	=	tip-sample distance
DI	=	deionized
ECM	=	extracellular matrix
E_i	=	Young's modulus of indenter
E_s	=	Young's modulus of sample
F	=	tip-sample force
FBS	=	fetal bovine serum
FDA	=	Food and Drug Administration
FTIR	=	Fourier transform infrared
Gly	=	glycine
HA	=	hydroxyapatite
H_2O_2	=	hydrogen peroxide
K	=	reduced elastic modulus
k_c	=	spring constant
LbL	=	layer-by-layer
LiBr	=	lithium bromide
M	=	molar
MPS	=	sodium 3-mercapto-1-propanesulfonate
n	=	number of quad-layer

LIST OF ABBREVIATIONS AND SYMBOLS (cont.)

NaCl	=	sodium chloride
NaOH	=	sodium hydroxide
Na_2CO_3	=	sodium carbonate
NH_4OH	=	mmonium hydroxide
OWRK	=	the Owens, Wendt, Rabel and Kaelble
PBS	=	phosphate buffer solution
PDDA	=	poly (diallyldimethylammonium chloride)
QCM	=	quartz crystal microbalance
R	=	tip radius
RCA	=	Radio Corporation of America
RGD	=	arginine-glycine-aspartic acid
rpm	=	revolutions per minute
SEM	=	scanning electron microscopy
Ser	=	serine
SF	=	silk fibroin
SFE	=	surface free energy
Ti	=	titanium
υ_i	=	poisson ratio of indenter
υ_s	=	poisson ratio of sample
WST-1	=	water-soluble tetrazolium salt
Z	=	the rest position of cantilever-sample distance
Δf	=	frequency shift
α-MEM	=	alpha-Minimum Essential Medium
γ_L	=	surface tension
γ_L^d	=	dispersive component of surface tension
γ_L^p	=	polar component of surface tension
γ_s	=	solid surface free energy
(γ_s^d)	=	dispersive component of solid surface energy
$\left(\gamma_s^p\right)$	=	polar component of solid surface energy

LIST OF ABBREVIATIONS AND SYMBOLS (cont.)

δ_c = cantilever deflection

CHAPTER 1

INTRODUCTION

1.1 Background and Motivation of the Research

In the past two decades, the design and manufacture of advanced nanostructured materials at the molecular level have been of tremendous interest to the scientific and engineering communities for their application in the biomedical field (Gentile et al., 2015). Among the available techniques, layer-by-layer (LbL) assembly has attracted considerable attention due to several advantages. A primary advantage of the LbL self-assembly technique is its ability to coat thin films with ordered structure in nanometer thickness range on supports of various shapes and sizes (Ai et al., 2003). Furthermore, the unique advantages of LbL for biomedical applications are shown outstanding in its ease of preparation and versatility; it also possesses the capability of incorporating high loadings of different types of biomolecules in the films.

Generally, the LbL self-assembly process involves the sequential exposure of electrostatic interactions between two oppositely charged polyelectrolytes that are alternately deposited onto charged solid surfaces. The adsorption steps can be repeated for several times to obtain the desired number of coating layers (Xiao et al., 2016). This technique is capable of fabricating multilayer coatings at controlled thickness at the nanometer scales.

Owing to the rapid development of assembly technologies of LbL self-assembly technique, LbL assembly strategies for tissue engineering has emerged as an alternative technique to repair and restore function of damaged or diseased tissues. This research topic is growing quickly in the clinical fields, particularly the clinical applications of tissue engineering in dental implantology (Sammartino et al., 2016).

Dental implants have become a more common form of treatment for the replacement of missing natural teeth. Dental implants not only look and function like natural teeth; they also support long-term oral health. However, not all dental implant surgeries are successful, with implant failure occurring in some cases. Lack of

osseointegration is one of the significant factors leading to primary implants failure due to the loosening of an implant in the bone (Kate et al., 2017). Osseointegration is a direct structural and functional connection between the implant surface and newly formed bone (Albrektsson and Jacobsson, 1987). There are many factors to achieve osseointegration, such as the biocompatibility of the implant material, implant surface, implant design, surgical approach and condition of the patient (Yang et al., 2006; Nijhawan et al., 2010). One strategy to improve osseointegration is modification of the implant surface, which can stimulate peri-implant bone formation and achieve faster osseointegration (Ting et al., 2017; Meng et al., 2016).

Dental implant surface technologies have advanced rapidly in the last decade. Surface modifications by coating with organic components of the extracellular matrix (ECM) like collagen type I have become interesting for enhancing bone formation on the implant surface due to active support of cell proliferation, adhesion, migration, and survival (Kim et al., 2011; Novales Jr. et al., 2010). Collagen, which constitutes the main structural component of ECM, displays excellent biocompatibility, regulation of cell adhesion, biodegradability, and direct tissue development (Parenteau-Bareil et al., 2010; Frantz et al., 2010). Type I collagen is the most abundant collagen form found in connective tissues including the skin, bones, tendons, and cartilage. Type I collagen also contains some specific amino acid sequences of arginine-glycine-aspartic acid (RGD), making it effective for promoting cellular adhesion and spreading along with tissue regeneration (Taubenberger et al., 2010; Yamada et al., 2014). Even though collagen has several advantages, a pure collagen scaffold is limited by low mechanical strength and fast degradation speed rate (Yamada et al., 2014; Sun et al., 2014). To overcome these disadvantages, collagen has often been used in combination with other biomaterials to effectively improve the mechanical properties of the scaffold (Ficai et al., 2010).

A combination of collagen and silk fibroin may result in composite materials with effective improvement of characteristics while simultaneously retaining the biocompatibility of the material. Silk fibroin, a natural protein spun by silkworms (*Bombyx mori*), has been investigated extensively as a biomaterial for biomedical applications. Silk fibroin presents several interesting properties such as excellent mechanical properties, biocompatibility and slow degradation (Sun et al., 2014;

Rockwood et al., 2011). Specifically, silk fibroin shows an excellent combination of strength and toughness which provides space maintenance for bone ingrowth while preventing membrane collapse (Kim et al., 2005; Rising et al., 2005). Silk-based biomaterials as tissue engineering scaffolds have been used to enhance bone regeneration and maintaining stability during bone regeneration.

In the application of LbL assembled films as biomedical materials, biocompatibility of polyelectrolyte materials is a major concern. In addition to natural polymers such as collagen and silk fibroin, poly (diallyldimethylammonium chloride) (PDDA) can also be used as the polycation for electrostatic LbL preparation of multilayer films due to its biocompatibility, high charge density and homogeneous distribution of positive charges (Sanches et al., 2015; Zhang et al., 2007). Furthermore, PDDA's unique structure gives it high water solubility and strong cationic electrolytic properties that enable easy interaction with anionic molecules (Ahn et al., 2011). These advantages contributed to the selection of PDDA as the base polymer for the fabrication of LbL self-assembled film in this research.

This research focuses on fabricating effective multilayer film onto glass slides by the LbL self-assembly technique and makes use of silk fibroin (SF) and type I collagen (Col) solutions as anionic polyelectrolytes, and alternately assembled using strong cationic PDDA. The characterization of the topographical structure, surface properties, and biological function is considered in this research. This research sought to evaluate how bifunctionality can be enhanced in the design of coated dental implant materials. It was expected that a combination of these biopolymers obtained $[PDDA/SF/PDDA/Col]_n$ multilayer film with excellent osseointegration characteristics for application as a dental implant material.

1.2 Objectives of Research

The objectives of this study are the following:

(1) To fabricate multilayer film based on silk fibroin and type I collagen for dental implant materials.

(2) To investigate the morphological, physical and cell supporting properties of multilayer film.

(3) To propose feasibility for enhancing the performance of multilayer film for dental implant applications.

1.3 Thesis Outline

The thesis consists of five chapters. In the present chapter, the statement of the problem is addressed, including the research objectives.

Chapter 2 presents biomaterials for used as scaffolds in tissue engineering and an overview of the LbL self-assembly technique.

Chapter 3 describes the preparation and fabrication of silk fibroin and type I collagen by LbL self-assembly technique in the forms of multilayer films for tissue engineering.

Chapter 4 describes the investigations of the morphological and physical properties of multilayer film and biological responses of osteoblast cell.

Chapter 5 summarizes the conclusion based on the results obtained from all presented studies and propose avenues for future research.

CHAPTER 2

THEORETICAL BACKGROUND

This chapter provides the necessary background of thesis. This includes the theoretical background of tissue engineering, the review of natural polymer for implant surface modifications and their properties. Several techniques for thin film coating of natural polymer multilayer films are also presented in this chapter.

2.1 Introduction to Tissue Engineering

Tissue engineering is an interdisciplinary field that applies the principles of the life sciences and medicine with those of engineering to building tissue and organs with cells and matrix materials for damaged tissue (Feldman, 2018). The goal of tissue engineering is the development of biological substitutes that maintain, improve or restore tissue function (Castells-sala and Recha, 2013).

Over the last few years, different types of materials, i.e. metals, ceramics, polymers, and composites have been investigated for the purpose of tissue engineering. The synthetic and natural polymers have been found to be suitable for use as tissue engineering scaffolds. Though synthetic polymers offer flexibility in processing and modification, they often suffer from associated disadvantages such as inflammation, immune reactions, and toxicity in humans. Therefore, natural polymers are gaining interest among the research community for tissue engineering application.

2.1.1 Tissue engineering of bone

The concept of bone tissue engineering began in the early 1980s. During the past few decades, tissue engineering has emerged as an alternative technique to repair and restore function of damaged or diseased tissues (Ueda, 2011). Bone is a mineralized connective tissue that exhibits four types of cells: osteoblasts, bone lining cells, osteocytes, and osteoclasts. Bone is a composite material consisting of both inorganic and organic components. The inorganic component is primarily crystalline

hydroxyapatite which constituent by weight about 60% of the tissue. The organic component of bone (approximately 30%) comprises collagenous proteins, predominantly type I collagen (90%), and non-collagenous proteins including osteocalcin, osteonectin, osteopontin, fibronectin and bone sialoprotein II, bone morphogenetic proteins (BMPs), and growth factors. The remaining 10% is water (Florencio-silva et al., 2015).

Bone tissue engineering is based on the understanding of bone structure, bone mechanics, and tissue formation as it aims to induce new functional bone tissues that enhance bone repair and regeneration (Amini et al., 2013). In general, bone tissue engineering consists of three basic elements, namely the cells, the growth factors (such as bone growth factor, bone inducing factor, etc.), and the bone scaffolds (Wu et al., 2017). The structure will be provided on the support which is called as a scaffolding. A scaffold can serve as a temporary ECM to support three-dimensional bone tissue regeneration. It is often beneficial for the tissue-engineering scaffold to mimic or replicate certain advantageous features of the natural ECM (Dang et al., 2018).

Numerous scaffolds produced from a variety of biomaterials have been used in designing scaffolds for bone engineering: synthetic polymers such as poly (α-hydroxy) acids and polyurethane foams; natural biopolymers such as collagen, silk fibroin, cellulose, chitosan, alginate, starch and hyaluronic acid; and ceramics such as hydroxyapatite and β-tricalcium-phosphate (Boschetti et al., 2008). There are several requirements in the design of scaffolds for tissue engineering. These requirements are as follows (Ghassemi et al., 2018; Fergal, 2011): 1) Biocompatibility in terms of cell attachment and proliferation as well as lack of toxicity. After implantation, the scaffold must elicit a negligible immune reaction in order to prevent it causing such a severe inflammatory response that it might reduce healing or cause rejection by the body. 2) Biodegradability for producing the body's own cells to replace the implanted scaffold or tissue engineered construct. The by-products of this degradation should also be non-toxic and able to exit the body without interference with other organs. 3) Mechanical properties appropriate to the anatomical site and strong enough to allow surgical handling during implantation. 4) Scaffold architecture for tissue engineering should have an interconnected pore structure and high porosity to ensure cellular penetration and adequate diffusion of nutrients to cells within the construct and the

ECM formed by these cells. 5) Manufacturing technology should be cost effective and it should be possible to scale-up from making one at a time in a research laboratory to small batch production.

2.1.2 Collagen for tissue engineering

In mammals, collagen is the most abundant protein, which constituting about 30% of the whole body protein content (Song et al., 2019). Collagen is a primary component of the extracellular matrix (ECM), serving as a physiologically active component of living tissue, responsible for cell-cell communication, cell adhesion, and cell proliferation (Walker et al., 2018). Collagen has potential as a biomaterial for bone tissue engineering due to its abundance, biocompatibility, high porosity, facility for combination with other materials, easy processing, hydrophilicity, low antigenicity and absorbability in the body (Ferreira et al., 2012). However, collagen has one major disadvantage in that it's high degradation rate, which results in a rapid loss of mechanical properties. Obviously, collagen has more advantages than disadvantages as shown in Table 2.1, that summarizes the major characteristics of collagen for tissue engineering applications. (Sahithi et al., 2013; Lee et al., 2001)

Generally, collagen has a polypeptide molecular structure built of amino acid monomers, called alpha chain (α-chain). Each α-chain composes of approximately 1,000 amino acids residues and varies in amino acid composition (Gordon and Hahn, 2010). Various types of collagen are classified and described as shown in Table 2.2 (Gelse et al., 2003), which characterizes their structure and supramolecular organization. Among these, type I collagen (Col) has been found as the most prevalent type in ECM. It forms more than 90% of the organic mass of bone and is the major collagen in connective tissue such as tendons, skin, ligaments, and cornea (Gelse et al., 2003). The structure of Col is arranged in the form of a long triple helix by two identical α1-chains and one α2-chain, as shown in Figure 2.1. The three polypeptide chains also called collagen monomer or tropocollagen, are held together by hydrogen bonds between chains and formed a rope-like structure, which has great tensile strength. The sequence of each α-chain is a repeat of the tripeptide Gly-X-Y, where Gly is glycine, X is often proline and Y is usually hydroxyproline.

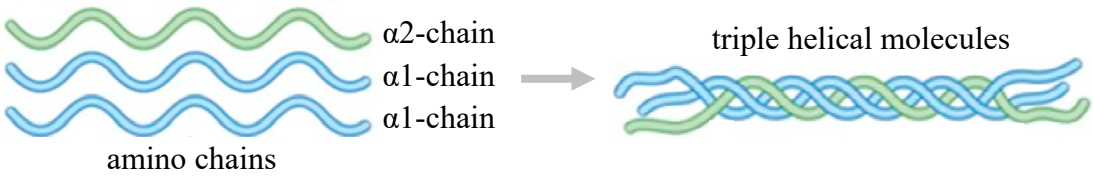

Figure 2.1 Structure of collagen triple helix.

Table 2.1 Advantages and disadvantages of collagen as biomaterial.

Advantages	Disadvantages
- No antigenicity - Non- toxic biopolymer - Better biocompatibility - Compatible with synthetic polymers - Hemostasis in nature and encourage blood coagulation - Existing in plenty and simply purified from living organisms - Synergism with other bioactive compounds - Absorbability on biological membranes - Easily modified to produce desired materials - Formulated in a number of different forms - Compatible with synthetic polymer - Positive effect on wound healing rates	- Rapid degradation rate - Poor of mechanical strength - High cost of pure type I collagen - Complex handling properties - Hydrophilicity causes swelling in water - Variability of isolated collagen (e.g. crosslink density, fiber size, trace impurities, etc.) - Variability in enzymatic degradation rate as compared with hydrolytic degradation

Table 2.2 The various collagen types as they belong to the major collagen families.

Type	Molecular composition	Tissue distribution
Fibril-forming collagens		
I	$[\alpha1(I)]_2\ \alpha2(I)$	bone, dermis, tendon, ligaments, cornea
II	$[\alpha1(II)]_3$	cartilage, vitreous body, nucleus pulposus
III	$[\alpha1(III)]_3$	skin, vessel wall, reticular fibers of most tissues (lungs, liver, spleen, etc.)
V	α1(V)α2(V)α3(V)	lung, cornea, bone, fetal membranes; together with type I collagen
XI	α1(XI)α2(XI)α3(XI)	cartilage, vitreous body
Basement membrane collagens		
IV	$[\alpha1(IV)]_2\ \alpha2(IV)$	basement membranes
Microfibrillar collagen		
VI	α1(VI)α2(VI)α3(VI)	widespread: dermis, cartilage, placenta, lungs, vessel wall, intervertebral disc
Anchoring fibrils		
VII	$[\alpha1(VII)]_3$	skin, dermal - epidermal junctions; oral mucosa, cervix
Hexagonal network-forming collagens		
VIII	$[\alpha1(VIII)]_2\ \alpha2(VIII)$	endothelial cells, Descemet's membrane
X	$[\alpha3(X)]_3$	hypertrophic cartilage
fibril-associated collagens		
IX	α1(IX)α2(IX)α3(IX)	cartilage, vitreous humor, cornea
XII	$[\alpha1(XII)]_3$	perichondrium, ligaments, tendon
XIV	$[\alpha1(XIV)]_3$	dermis, tendon, vessel wall, placenta, lungs, liver
XIX	$[\alpha1(XIX)]_3$	human rhabdomyosarcoma
XX	$[\alpha1(XX)]_3$	corneal epithelium, embryonic skin, sternal cartilage, tendon
XXI	$[\alpha1(XXI)]_3$	blood vessel wall
Transmembrane collagens		
XIII	$[\alpha1(XIII)]_3$	epidermis, hair follicle, endomysium, intestine, chondrocytes, lungs, liver
XVII	$[\alpha1(XVII)]_3$	dermal – epidermal junctions
Multiplexins		
XV	$[\alpha1(XV)]_3$	fibroblasts, smooth muscle cells, kidney, pancreas
XVI	$[\alpha1(XVI)]_3$	fibroblasts, amnion, keratinocytes
XVIII	$[\alpha1(XVII)]_3$	lungs, liver

2.1.3 Silk fibroin for tissue engineering

Silk fibroin (SF), which is secreted by silkworms, spiders, mites, and pseudo-scorpions (Im et al., 2016), is a natural fibrous polymer with strong potential for many biomedical applications. SF has attracted interest in the field of bone tissue engineering due to its extraordinary characteristics in terms of elasticity, flexibility, biocompatibility, and biodegradability (Farokhi et al., 2018). Moreover, SF possesses extraordinary properties for stimulating bone repair; for example, the fibrous structure of SF is mostly similar to Col. Furthermore, SF properties are shown outstanding in its slow rate of degradation and low immunogenicity; it also possesses excellent mechanical strength, and suitable processability makes it a useful scaffold system for various tissue engineering applications, including bone substitute and bone constructs. Until now, many studies have explored potentials of SF-based biomaterials both in *vitro* and *vivo* for the engineering/regeneration of a variety of tissues including bone, cartilage, ligament, tendon, muscle, etc. (Figure 2.2). Particularly, bone tissue showed the maximum percentage of various tissues based on detailed analysis of the number of publications and citations on the use of SF as scaffold for tissue engineering (Ma et al., 2018).

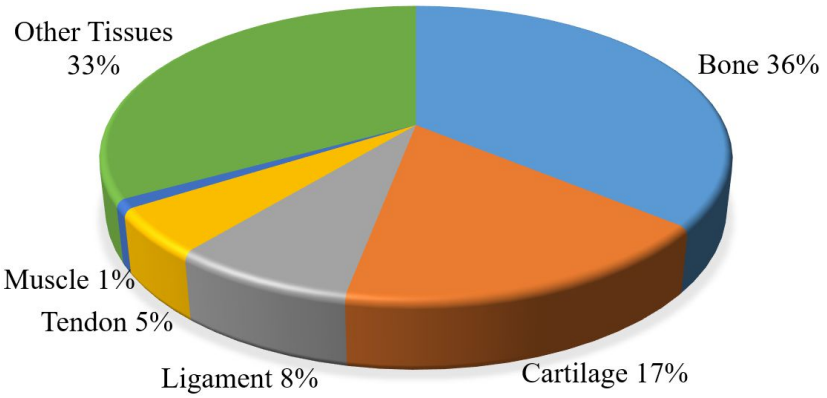

Figure 2.2 Relative percentage on silk-based in vitro engineering of various tissues.

Silkworm silk is a kind of natural protein fiber. The silk proteins of silkworm are synthesized specifically by the silk gland, which is composed of two types of proteins: fibroin (70%–80%) and sericin proteins (20%–30%). SF is composed of 18 amino acids. Almost 80% of total amino-acids are glycine (Gly), alanine (Ala) and serine (Ser) (Li et al., 2013). The amino acid sequence of SF contains repetitive Gly-Ala-Gly-Ala-Gly-Ser (GAGAGS) repeats and forms the antiparallel β-sheet structure in the spun fibers, which is responsible for its good mechanical properties (Zafar and Al-Samadani, 2014). Among various types of silk fibers, *Bombyx mori* (*B. mori*) is one of the best characterized which is also known as mulberry silk.

Currently, *B. mori* silk fiber is mainly used as textiles for textile industries, tissue engineering and suture material in biomedical industries. *B. mori* silk fiber is naturally created with two different protein-based layers as shown in Figure 2.3, fibroin in an inner layer and a sericin coating in an outer layer (Ude et al., 2014). The *B. mori* silk fibroin is composed of two protein chains, heavy-chain (H-fibroin) and light chain (L-fibroin) with the molecular weight of approximately 350 kDa and 26 kDa respectively, covalently linked by a disulfide bond at the carboxy-terminus of the two subunits, forming an H-L complex. A glycoprotein P25 (~25 kDa) is also non-covalently linked to the H-L complex. The H-chain, L-chain, and P25 are assembled in a ratio of 6:6:1 to form silkworm silk (Liu and Zhang, 2014).

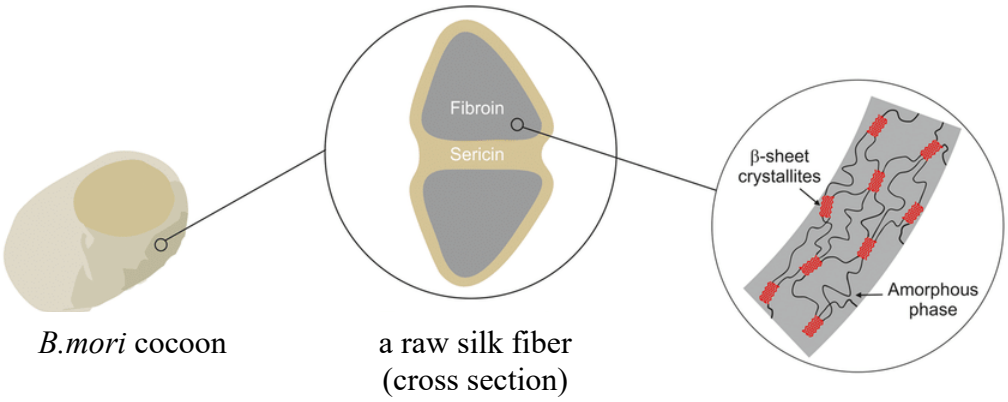

Figure 2.3 Schematic of the main components of *B. mori* cocoon.
(Susana et al., 2016)

SF, a natural multi-domain protein, was recognized by the US Food and Drug Administration (FDA) as a biomaterial in 1993. SF has attracted great attention due to its superior mechanical properties such as ultra-high strength and stretchability, biocompatibility, as well as its versatile biodegradability and processability. SF can be processed into various forms of SF-based biomaterials such as nanofiber, gel, and film (Qi et al., 2017). Importantly, SF has predominant mechanical properties over the other biological materials as Table 2.3 (Liu and Zhang, 2014; Ude et al., 2014; Blackledge and Agnarsson, 2010). Therefore, it is often used in a scaffold for tissue engineering. In addition to these advantages, SF also has disadvantages such as lack of biological functions (Jung et al., 2014) and poor hemocompatibility (Elahi et al., 2014). Table 2.4 showed summarizes the advantages and disadvantages of silk as biomaterial for tissue engineering applications.

Table 2.3 Comparison of mechanical properties of natural silks and other materials.

Materials	Strength (MPa)	Stiffness (GPa)	Toughness (MJ m^{-3})
B.mori silk (with sericin)	500	5–12	70
B. mori silk (without sericin)	610–690	15–17	70–78
Spider silk	875-972	11-13	111-160
Collagen	0.9-7.4	0.0018-0.046	-
Bone	160	20	4
Tendon	150	1.5	12
Elastin	2	0.001	2
Resilin	3	0.002	4
Synthetic rubber	50	0.001	850
Polylactic acid	28-50	1.2-3.0	1-3
Nylon fiber	950	5	80
Kevlar 49 fiber	3600	130	50

Table 2.4 Advantages and disadvantages of silk as biomaterial.

Advantages	Disadvantages
- Excellent mechanical properties - Environmental stability - Nontoxic and good biocompatibility - Versatility of structural re-adjustments - Collaborate with bioactive components - Fabricated to variety of form - slow degradation rate and retaining strength long term to applied in medical application such as sutures	- Lack of biological function - Poor hemocompatibility - Side effects from silk sericin induced Type I allergic response

2.2 Osseointegration of Dental Implants

Dental implantology, a special field of dentistry dealing with the rehabilitation of the damaged chewing apparatus due to loss of the natural teeth, is currently the most intensively developing field of dentistry. Missing teeth can be replaced by dental implants (artificial roots), which are inserted into the root-bearing parts of the mandible or maxilla. The success rate and long-term prognosis of such implants have also depended primarily on the anchorage of the implant in the jawbone. The end of this bone healing process is called osseointegration. This process of osseointegration depends not only on implant-related factors such as material, shape, topography and surface chemistry but also on mechanical loading, surgical technique and patient variables such as bone quality and quantity (Vootla and Reddy, 2017). However, dental rehabilitation with conventional prostheses is often unsuccessful because of the altered oral anatomy and the lack of adequate dentition for fixation (Pellegrino et al., 2018).

Osseointegration was first described by Branemark (1983) as direct contact between living bone and a loaded implant surface at a histological level (Bernhardt et al., 2012). There are many factors affecting osseointegration such as

implant biocompatibility, design characteristics, implant surface, state of the host bed, surgical technique and the loading conditions. It is well established that characteristics of implants surface have a major influence on the outcome of osseointegration (Ramazanoglu and Oshida, 2011). Several surface modification techniques have been used to generate topographical cues on the implant surface in order to enhance osseointegration, which can stimulate peri-implant bone formation and achieve faster.

2.3 Implant Surface Modifications on Osseointegration

The osseointegration process relates to all biological interactions between the host bone and implant surface. Following the placement of the implant, primary implant stability is achieved by passive mechanical fixation within the host bone. There is a predictable sequence of bone turnover and replacement at the interface that allows the newly formed bone to adapt to microscopic roughness on the implant surface, and even a nanotopography has been shown to preferably influence the formation of bone. As such, surface modification is usually performed to improve the biological, chemical, and mechanical properties. Currently, different materials, implant surface treatments, and coatings have been proposed to enhance clinical performance.

To promote osseointegration achieve faster and stronger bone formation, the development of implant surface modifications is the main objective. Topographical modifications may enhance short- and long-term osseointegration and healing (Eldo and Sunitha, 2015). There are numerous reports, demonstrate that surface roughness of implant also has a positive influence on cell response, which achieves better bone-to-implant contacts results (Dahiya et al., 2014). Furthermore, the wettability of the surface also plays an important role with respect to cell attachment and spreading (Frank et al., 2015). Therefore, the surface characteristics of the implant, such as roughness, wettability, the chemical properties, and so on are parameters that may play a role in implant-tissue interaction and osseointegration.

2.3.1 Topography and roughness of implant surface

The characteristics of implant surface topography and roughness have received great deal attention in recent years. Various studies point out that when the surface roughness of the implant is incremented, this will improve osteoblast response in vitro and osseointegration in vivo (Solá-Ruiz et al., 2015; Ma et al., 2016). Therefore, surface topography and roughness can be considered a very influential surface property for conditioning the response of the organism to achieve favorable interaction between the implant and biological tissues.

Based on the dimension of the measured surface features, the surface roughness of implant topography can be classified into macro-, micro-, and nanoscale-sized topologies (Dahiya et al., 2014; Alla et al., 2011).

1) Macro-roughness directly relates to implant geometry, with a threaded screw and macroporous surface treatments in the range of millimeters to tens of microns. Macro-sized topographies with high rough surfaces help in initial implant stability and provide volumetric spaces for growth of bone. However, high surface roughness may result in an increase in ionic leakage as well as peri-implantitis. Therefore, dental implantology was mainly focused on micro- and nanogeometry.
2) Micro-roughness comprises features in the range of 1-10 μm. This range of roughness attempts to enhance the osteoconduction (in-migration of new bone) and osteoinduction (new bone differentiation) along the implant surface. The study of Pieles et al. (2007) has examined the effect of the implant surface on bone healing showing a significantly greater percentage of bone-to-implant contact for micro-rough titanium surfaces compared with polished titanium surfaces.
3) Nano-roughness is composed of nano-sized materials with scale range from 1 to 100 nm. Nanotopography of dental implants is an influence on cell-implant interactions at the cellular and protein level. Changes in nanotopography convey their effects on surface

energy, resulting in increased adhesion of osteogenic cells and thereby potentially promoting osseointegration (Smeets et al., 2016).

2.3.2 The surface wettability

One of the important factors influencing bone-to-implant contact is surface wettability. Wettability is dependent on surface energy, which increases the osteoblasts cell adhesion on the implant surface. (Lawande and Lawande, 2016). This property presents major advantages during the initial stages of wound healing and during the cascade of events that occurs during osseointegration, facilitating bone integration. The degree of contact angle which the primary physical parameter is first presented by Thomas (1805). Generally, the hydrophilic surface is defined as a contact angle of less than 90°, while a surface with a contact angle more than 90° is hydrophobic. (Ma et al., 2016).

The surface energy of an implant, measured in directly by the liquid-solid contact angle and thus related to wettability, is another surface characteristic known to affect the biological response to the implant. Most studies have found that hydrophilic surfaces tend to enhance the early stages of cell adhesion, proliferation, differentiation, and bone mineralization compared to hydrophobic surfaces. However, opposite results have been found in studies using different chemistries, and it is possible that extremely high surface energies promote cell adhesion but hinder cell motility and subsequent cell functions (Gittens et al., 2014).

2.3.3 Methods of surface modification of implant

In recent years, with the technological development of implantology, techniques that shorten treatment time and lower failure risk are urgently demanded. Implant quality depends on the chemical, physical, mechanical and topographic characteristic of the surface. Implant surface modifications with several methods have been employed to change the implant surface morphology, chemistry, and structure (Lawande and Lawande, 2016). One of the most important surface properties is the topography of the surface. Topographical modifications may enhance short- and long-

term osseointegration and healing (Eldo and Sunitha, 2015). The desired implant surface can be achieved by the addition of material over the surface, removal of material from the surface or modification of the surface material. Surface modifications based on the deposition of coatings retain the mechanical properties of the implant material while the functionality of the implant surface can be upgraded by application of (bio)chemical compounds that act as cues towards improved bone regeneration (Bosco et al., 2012). Applying thin films to modified the surface properties of a biomaterial has been widely used onto different surfaces by several methods such as spin coating, dip coating, plasma spray coating, and LbL assembly; so on.

2.3.3.1 Spin coating

The spin coating process has been widely used to deposit uniform thin films on flat substrates. This method is extraordinary because of the merit of conveniences, reproducibility, use of low-cost equipment and fast operation speed. The film thickness is primarily controlled by solution viscosity, angular speed, and spin time. Figure 2.4 showed four steps summarized for the spin-coating method including deposition, spin-up, spin-off, and evaporation.

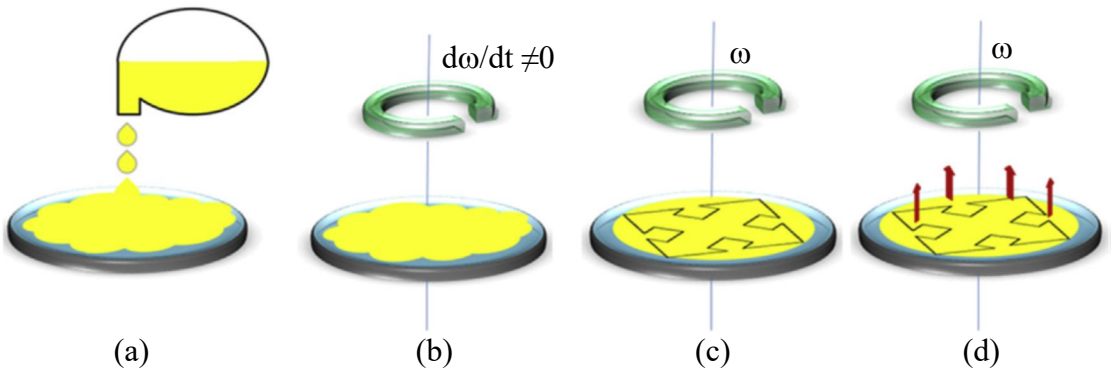

Figure 2.4 The different stages of spin coating. (a) Dispensation, (b) Acceleration, (c) Flow dominated, (d) Evaporation dominated. (Mozafari et al., 2016)

2.3.3.2 Dip coating

A dip coating process is one of the commonly used liquid-phase deposition methods for the formation of thin films. The technology of this process is based on dipping a substrate into a solution at a controlled rate. Dip coating is the easiest and fast method to prepare thin films from chemical solutions with the highest degree of control, making it highly appropriate for small scale production. The process of film formation in total implies several technical stages as demonstrated in Figure 2.5. Starting with the immersion of the substrate into the initial solution before withdrawing it at a constant speed. During the withdrawal process, a thin layer of the solution remains on the surface of the substrate. Once fully withdrawn, the liquid from the film begins to evaporate and leaves behind a dry film. Evaporation then takes over and leads to solidification of the final coating. For certain materials, a further curing step can be performed; this forces the deposited material to undergo a chemical or physical change.

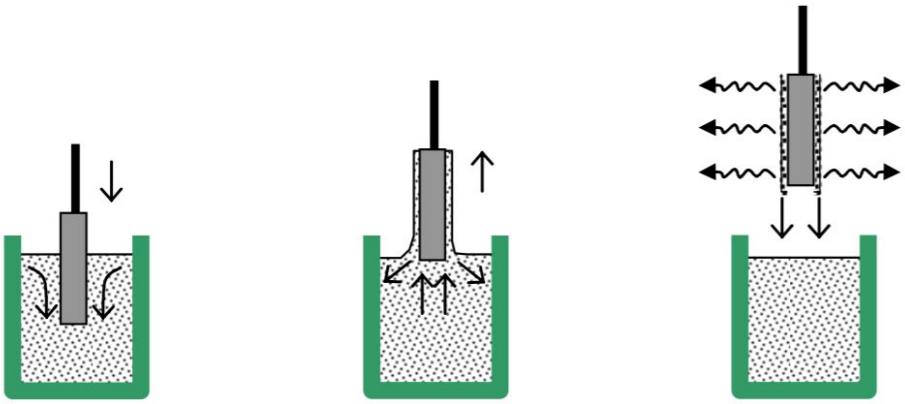

Figure 2.5 Scheme of the dip coating process. (Sánchez-Herencia, 2014)

2.3.3.3 Plasma spray coating

Plasma spraying technique generally involves a thick layer of depositions, such as hydroxyapatite (HA) and titanium (Ti). Plasma spraying method consists of injecting HA or Ti powders into a plasma torch at high temperature and

projected onto the surface of the implants where they condense and fuse together, forming a film (Figure2.6). The plasma spray substantially increased the surface area of the implants by increasing their surface roughness. This is advantageous as the coating gives implant a porous surface that the bone can penetrate more readily achieving faster osseointegration (Lawande and Lawande, 2016). However, this method is not very effective for coating tiny dental implants with a complex shape. One of the major concerns with plasma sprayed coatings is the possible delamination of the coating from the surface of the implant and failure at the implant-coating interface despite the fact that the coating is well-attached to the bone tissue (Le Guéhennec et al., 2007).

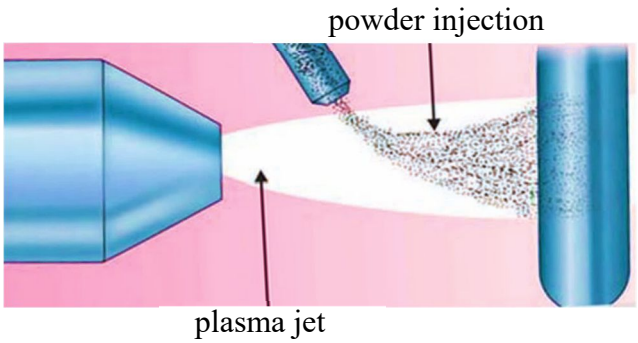

Figure 2.6 Process of a plasma spray. (Eldo and Sunitha, 2015)

2.3.3.4 Sol-gel technique

Among the various methods used to prepare thin films, sol-gel offers many advantages including low-temperature processing, a cost-effective and versatile technique, precise microstructural and chemical control, thickness control and surface finish of the coatings, ability to coat complex shapes high homogeneity and simplicity for full coverage of complex structures. The sol-gel-derived film or layer provides not only a good degree of biocompatibility but also a high specific surface area (which can be used as a carrier of adsorbed drugs) and an external surface whose rich chemistry allows ease of functionalization by suitable biomolecules (Owens et al., 2016).

However, this technique has its disadvantages. The major drawback of this process is the poor mechanical properties which the thin film is sensitive to heat treatment, resulting in cracking on the film layer. There is often a substantial volume

shrinkage and cracking during drying. Owing to the complexity of the procedure, coupled with the high costs of the raw materials (the chemicals) compared to other conventional techniques, sol-gel techniques are not used for large scale manufacture (Mallick and Winnett, 2014).

2.3.3.5 Layer-by-layer assembly

LbL assembly is a prevalent method for coating substrates with functional thin films. Generally, LbL assembly is a cyclical process that relies on electrostatic interactions between oppositely charged polyelectrolytes during sequential deposition onto a substrate, and after washing, an oppositely charged material is adsorbed on top of the first layer; however, a variety of other chemical interactions are also harnessed by LbL techniques such as hydrogen bonding and biomolecule recognition (Keeney et al., 2015).

Although electrostatic interactions remain widely used in facilitating the formation of thin films, the covalent and hydrogen bonding are currently well established for LbL formation. Furthermore, to achieve different applications, diverse materials such as polymers, proteins, lipids, nucleic acids, nanoparticles, and superstructure are also used as film constituents. The simplicity, versatility, and nanoscale control that LbL assembly provides make it one of the most widely used technologies for coating (Figure 2.7(a)). The widespread use of LbL assembly in fields with different standard tools and procedures; as well as the different processing requirements associated with substrates, has led to the development of a number of LbL assembly technologies (Figure 2.7(b)). The basis of LbL assembly is the sequential exposure of a substrate to the materials that will compose the multilayer films. The LbL coating can be performed using various methods, such as dip LbL, spray LbL, and spin LbL, etc. as shown in Figure 2.8.

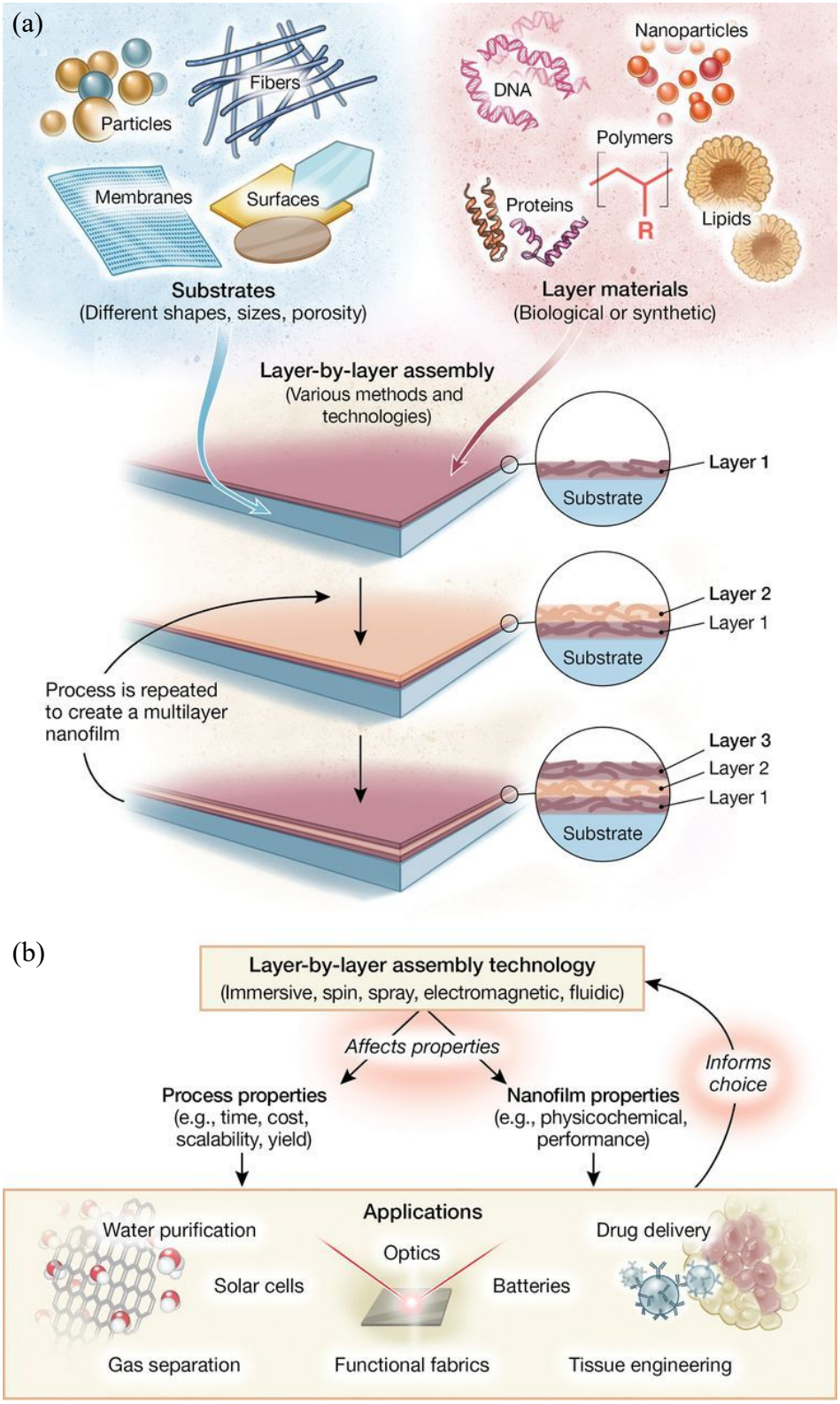

Figure 2.7 Versatility of LbL assembly. (a) Schematic overview of LbL assembly; (b) an overview showing that assembly technology influences film and process properties as well as application areas. (Richardson et al., 2015)

(a) Dip

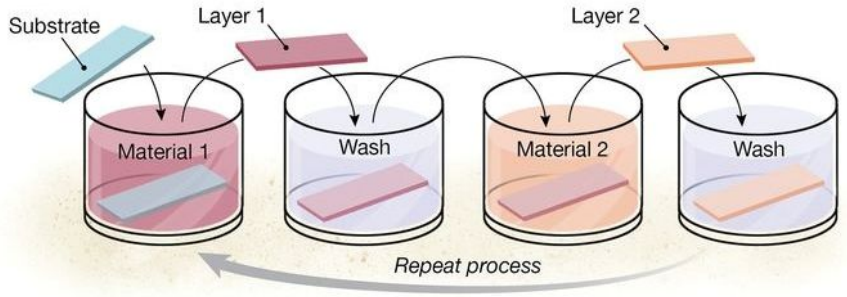

(b) Spin

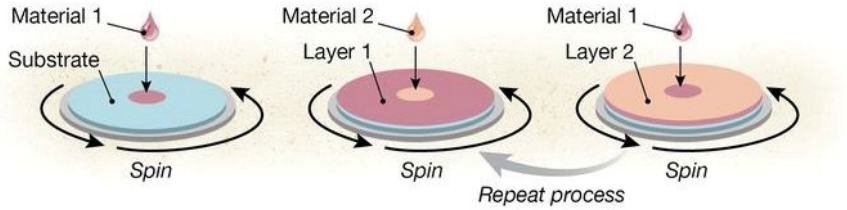

(c) Spray

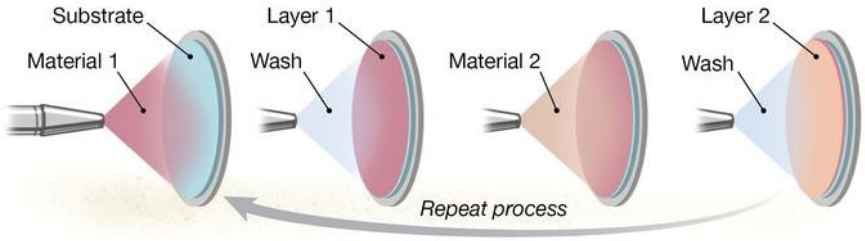

(d) Electromagnetic

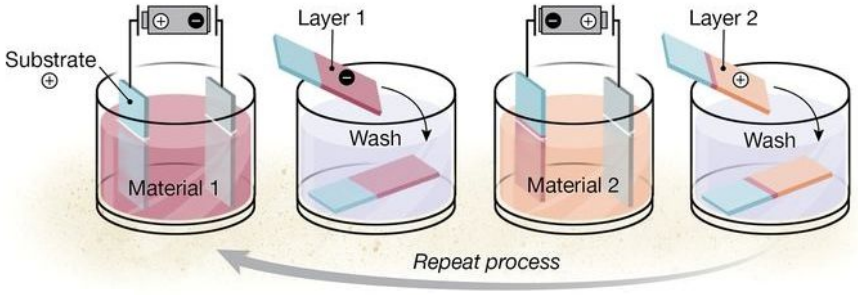

(e) Fluidic

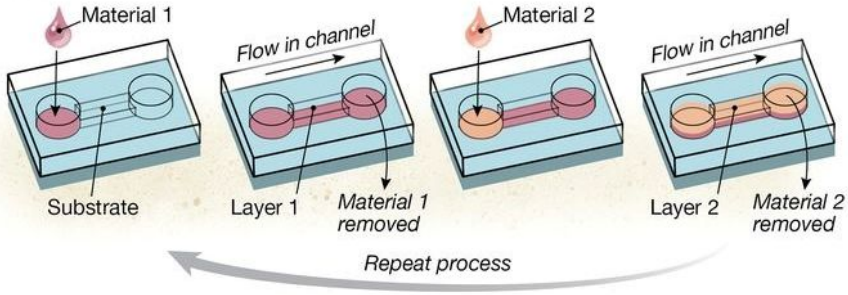

Figure 2.8 LbL assembly technologies. (a)-(e) Schematics of the five major technology categories for LbL assembly. (Richardson et al., 2015)

2.4 Layer-by-Layer Self-Assembly

2.4.1 The basic principle of LbL technique

Fabrication of functional thin films can be achieved via several deposition techniques as previously mentioned. Among all the techniques, LbL has several significant advantages that make this technique very useful for fabrication of functional thin films. The LbL assembly technique was first developed and introduced in 1966 by Iler (Iler, 1966). The method did not receive much credit nor attention from the scientific community until it was reintroduced in 1991 by Decher et al. as a solution for deposition of charged polymers (Gero et al., 1991; Ariga et al., 2010). Decher and colleagues exploited this method and prepared multilayers of thin films by immersing a charged planar surface (silicon wafer or quartz) alternately into anionic and cationic polyelectrolyte or bipolar ampholyte solutions. They used macroscopic planar silicon wafers and quartz surfaces, which are negatively charged, as the templates, and immersed the substrate initially into a solution containing a cationic polyelectrolyte. After that, a monolayer of polyelectrolyte was found to be adsorbed onto the surface of the solid. After rinsing, the solid was then immersed into another solution with an anionic polyelectrolyte. Again, a monolayer was adsorbed, and the original surface charge was restored. Since then, the method has developed rapidly as a very efficient, robust, and environmentally friendly surface treatment method.

The basic principle of the LbL method is to utilise electrostatic interactions between oppositely charged polyelectrolytes on a charged substrate. This process can be repeated to form any number of desired bilayers. The films generated from LbL depositions are relatively thin, around a few nanometers to a few micrometres thick depending on the number of bilayer, the pH, and the concentration of the polyelectrolyte solution (Michel et al., 2005). Figure 2.9 shows schematic of LbL self-assembly of a multilayer coating.

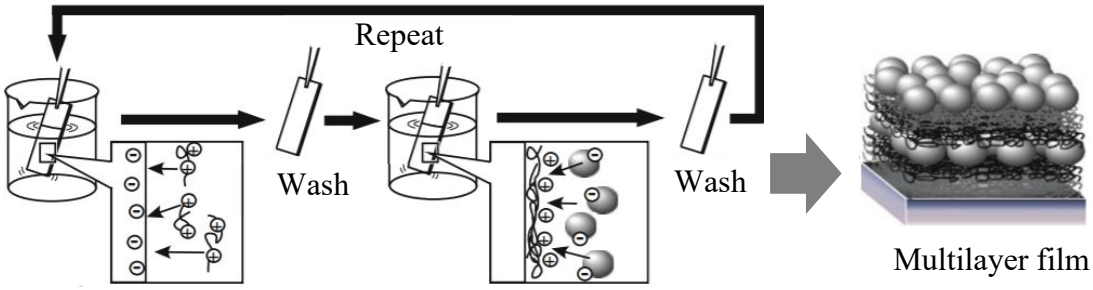

Figure 2.9 LbL self-assembly based on electrostatic interaction. (Ariga et al., 2010)

2.4.2 Methods operated in LbL Self-assembly

According to the LbL technique, the operating principle could be performed in several different approaches including spin LbL assembly, spray LbL assembly and dip LbL assembly. Each method has distinct advantages and disadvantages, which are summarized in Table 2.5. (Yusoff et al., 2018)

Table 2.5 Advantages and disadvantages for methods operated in LbL self-assembly.

Method	Advantages	Disadvantages
Dip LbL coating	- Simple method. - Very efficient. - Film produce more thicker, dense and smoother.	- Time consuming. - Risk of cross-contaminate.
Spin LbL coating	- Fast deposition. - Small amount polyelectrolyte. - Film produce more uniform, and smooth.	- Complex method. - Applicable only for small area.
Spray LbL coating	- Fast deposition. - Applicable for large area.	- Complex method. - Time consuming.

2.4.3 Advantages of LbL modified implant surface

LbL technique has many advantages. The LbL assebly process is simple and mild. This technique does not require special equipment. This coating method may be applied to control a biological response to the device such as peri-implant tissue formation since the polyelectrolyte multilayer is formed via electrostatic interactions between molecules under mild conditions, which could maintain their biological activity. Furthermore, the structure in the outer coating can be designed to incorporate additional biomolecules to control biomolecule release in field biomedical engineering (Keeney et al., 2015). Figure 2.10 shows a schematic illustration of LbL self-assembly coated titanium dental implant and localized delivery of substance to its surrounding environments to provide some benefit effects.

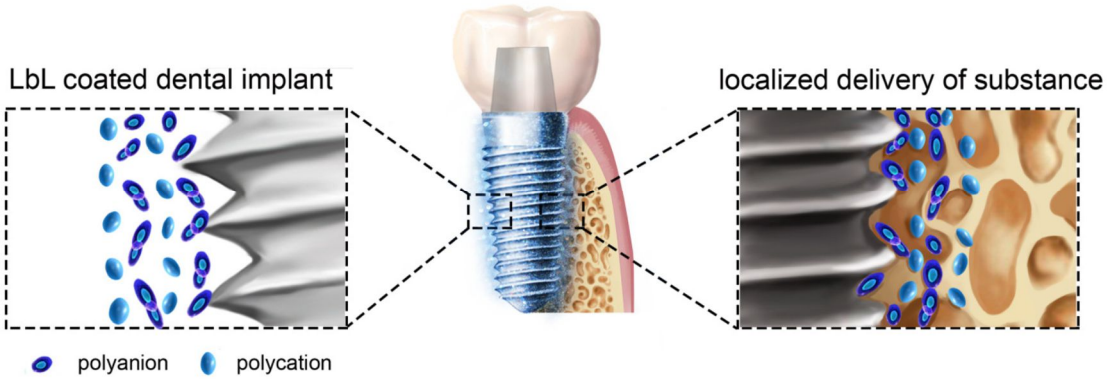

Figure 2.10 LbL coated titanium dental implant and localized delivery of substance to its surrounding environments to provide some benefit effects.
(Shi et al., 2017)

CHAPTER 3

RESEARCH METHODOLOGY

This chapter describes in detail the research methodology that is used within this research. The procedure will be provided describing how the implementation of the research was carried out, including data collection and data analysis.

3.1 Preparation of Aqueous Silk Fibroin Solution

Silk cocoons from *B. mori* were collected from Queen Sirikit Sericulture Center, Narathiwat, Thailand. SF was obtained by a degumming process (Figure 3.1). Briefly, raw silk cocoons were initially degummed by boiling in 0.02 M sodium carbonate (Na_2CO_3) solution for 30 min., rinsed thoroughly several times with deionized (DI) water to remove any sericin residual from the surface of the fiber. The obtained degummed fibers were dried at 60 °C overnight in the drying oven, and then it was dissolved in 9.3 M lithium bromide (LiBr) solution at 70 °C for 3 h. The dissolved SF was dialyzed in a cellulose dialysis membrane (MW3500, SpectraPor, USA) against DI water for 3 days with water changes every 6 h. The dialyzed SF solution was centrifuged at 9000 rpm for 20 min to remove insoluble particulates. The concentration of the SF aqueous solution was determined by weighing the remaining solid after drying divide by volume of SF and then stored at 4°C for further study.

For LbL dipping, 0.1 mg/mL SF solution was prepared by dissolving in DI water. DI water (resistivity 18.3 million ohm·cm) was purified with an E-Pure water purification system. The pH value was adjusted to 10 by adding sodium hydroxide (NaOH) and then filtered using a 4–12 μm membrane filter (Macherey-Nagel, MN615) prior to use. (Nawae et al., 2018)

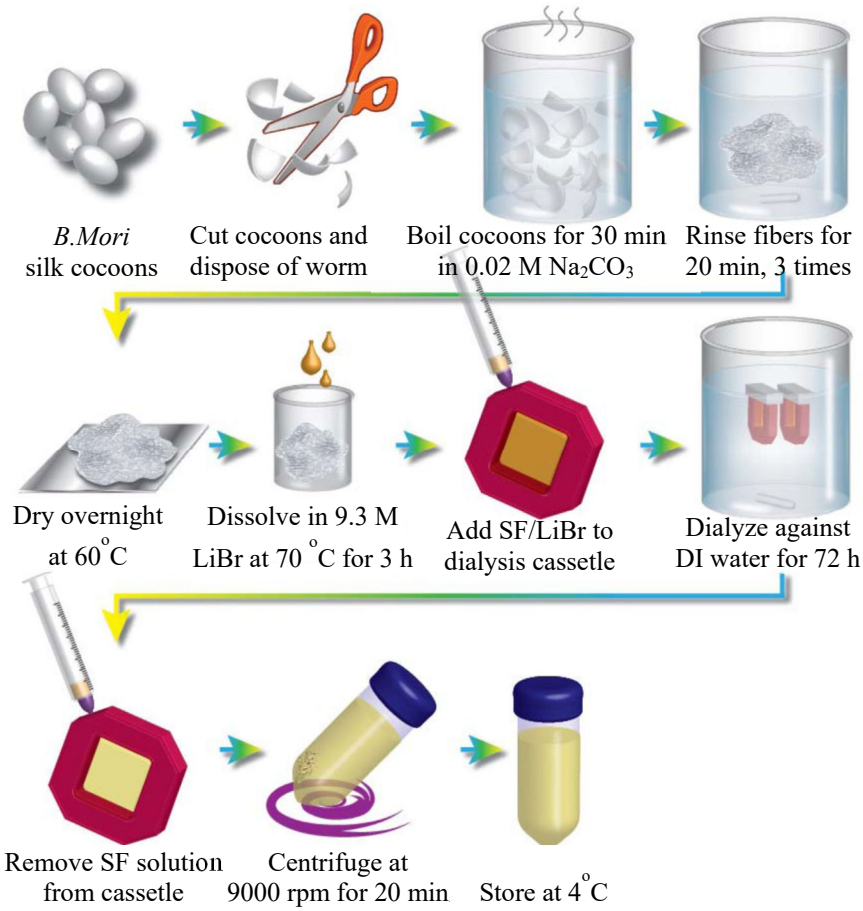

Figure 3.1 Schematic of the silk fibroin extraction procedure. (Rockwood et al., 2013)

3.2 Preparation of Type I Collagen

Type I collagen from the brown-banded bamboo shark (*Chiloscyllium punctatum*) skin was used for Col extraction. The Col was extracted and purified from shark skin according to the methods of Kittiphattanabawon et al. (2010), as shown in Figure 3.2. The skin was cleaned with cold water until any residual smell of ammonia disappeared. The clean shark skin was cut into small sizes (1.0 cm × 1.0 cm) and treated the deproteinized skin was washed thoroughly with cold water until the pH of wash water become neutral. The extraction was initially performed by soaking the pretreated skin in 0.5 M acetic acid solution for 2 days, followed by filtrating with two layers of cheesecloth. The Col solution was then precipitated by adding sodium chloride (NaCl)

to the final concentration of 2.6 M in the presence of 0.05 M tris(hydroxymethyl) aminomethane at pH 7.5 which was subsequently refrigerated to collect the precipitated Col pellet using a centrifuge machine. The obtained Col pellet was dissolved in a minimum volume of 0.5 M acetic acid and dialyzed with 0.1 M acetic acid for 12 hr and with DI water for 48 hr until a neutral pH was reached. All processes were performed at 4°C with gentle stirring. The resulted dialysate was finally freeze-dried to remove the water and it was kept in a sealed container at −20°C until further use.

For LbL dipping, the Col was solubilized in 0.1 M acetic acid at a concentration of 0.1 mg/mL. The pH value was adjusted to 10 by adding NaOH and then filtered using a 4–12 μm membrane filter (Macherey-Nagel, MN615) prior to use. (Nawae et al., 2018)

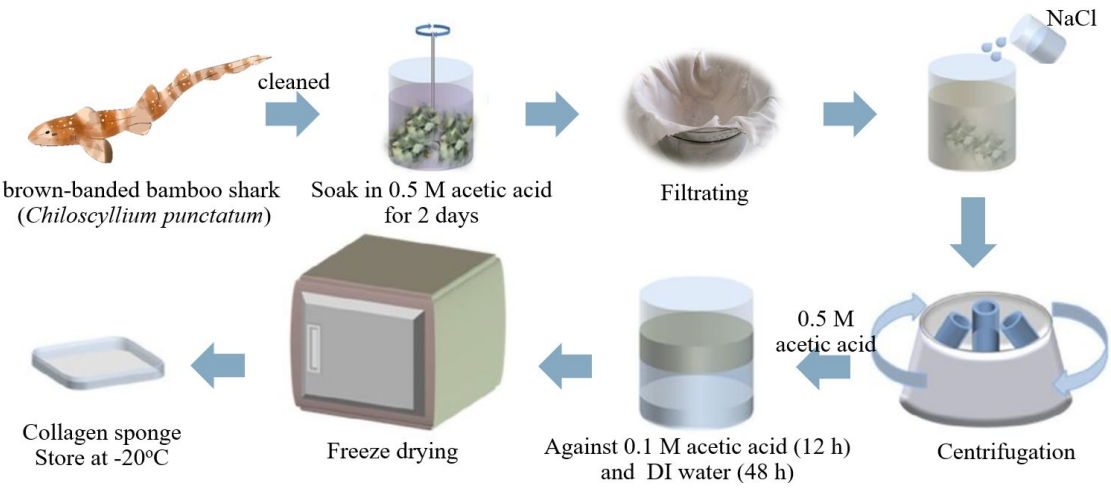

Figure 3.2 Schematic of the collagen extraction procedure.

3.3 Preparation of PDDA Solution

PDDA 20 wt% in water was purchased from Sigma-Aldrich Company (USA) and used as received without further purification. 0.01 M PDDA solution was prepared by dissolving in DI water, having a resistivity of 18.3 million ohm·cm, which was purified by an E-Pure water purification system. The pH of the solutions was adjusted to 10 by adding NaOH and then filtered using a 4–12 μm membrane filter (Macherey-Nagel, MN615). (Nawae et al., 2018)

3.4 Cleaning Processes Based on Hydrogen Peroxide

The substrate used in the experiments was a glass slide with dimensions of 25.4 mm x 76.2 mm. The pieces of glass slides were first cleaned with acetone followed by rinsing with DI water. The Radio Corporation of America (RCA) cleaning procedures were carried out next in order to remove contaminated organic compounds (Kern, 2006). This RCA solution was prepared by mixing ammonium hydroxide (NH_4OH), hydrogen peroxide (H_2O_2), and DI water in the ratio of 5:1:1. The glass slides were soaked in RCA bath at 70 °C for 15 min. After that, the glass slides were rinsed with DI water several times and blown dry with nitrogen flow at room temperature. With the RCA cleaning procedure, the surface became negatively charged and extremely hydrophilic due to the formation of hydroxyl and hydroxylate groups (Gorin et al., 2009; Kim et al., 2013).

3.5 Multilayer Film Preparation

Multilayer films were prepared on glass slides. The glass slides were cleaned using RCA solution according to the procedures mentioned above. The build-up of LbL self-assembly deposition is driven by electrostatic attraction between oppositely charged constituents. In this work, anionic molecules i.e., SF and Col were alternatively deposited on the prepared substrate between cationic PDDA molecule using an automatic dipping machine as illustrated in Figure 3.3. A negatively charged substrate was first immersed into PDDA solution for 3 min to form the positively charged monolayer. Next step was followed by a washing step in DI water for 2 min. Then, the monolayer-coated substrate was immersed into SF solution for 10 min, followed by the same washing procedure to remove unabsorbed polyelectrolytes and prevent cross-contamination of oppositely charged polyelectrolytes. Subsequently, the bi-layer coated substrate was again immersed into the PDDA solution for 3 min to permit adsorption of the opposite charge on the previously adsorbed SF layer. The tri-layer coated substrate was then washed and reversed to a negative charge by dipping into Col solution for 10 min. Washing was repeated as in the previous step, resulting in the formation of one quad PDDA/SF/PDDA/Col layer. The entire cycle was then

repeated until the desired number of quad-layer (n) were formed, designated as $[PDDA/SF/PDDA/Col]_n$.

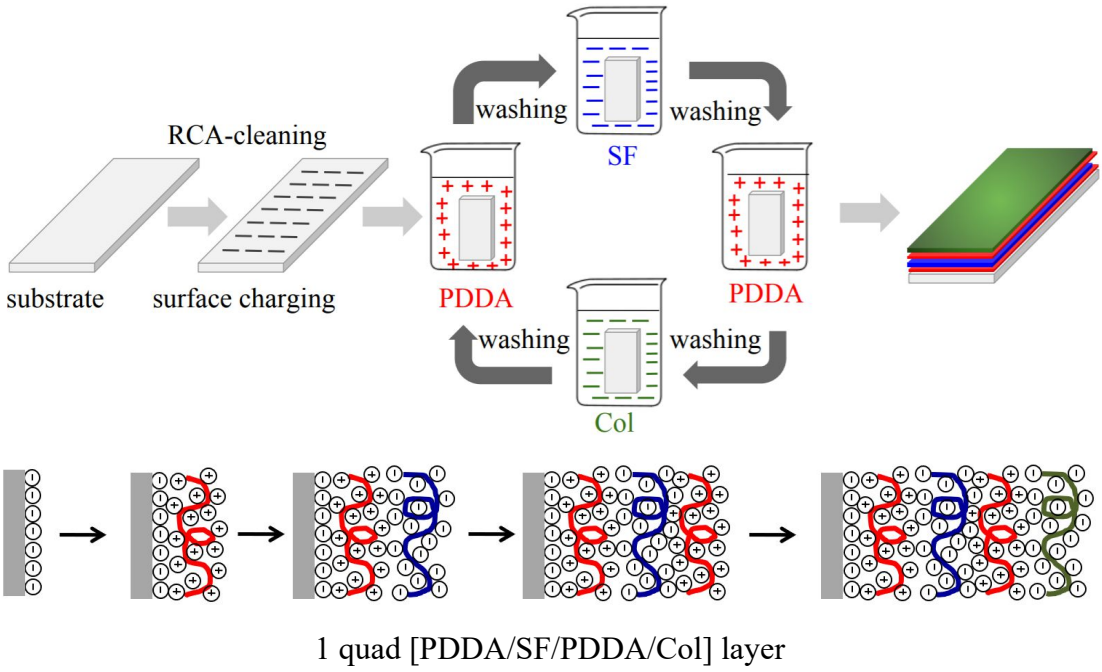

Figure 3.3 Schematic of 1 quad PDDA/SF/PDDA/Col LbL self-assembly formation on a glass slide surface.

3.6 The Quartz Crystal Microbalance Measurement

Quartz crystal microbalance (QCM) has been employed to monitor the real-time kinetics of the molecular binding of the multilayer assembly between the negatively- and positively-charged layers. The Monitoring self-assemble monolayer via QCM is an accurate yet inexpensive technique. The QCM measurement was performed on a QCM200 system (Stanford Research Systems Inc., SRS, USA) includes a 5 MHz, 1" diameter, AT-cut quartz crystal with circular polished gold electrodes on both sides (SRS #O100RX1). QCM measurement provides a 0.01 Hz frequency measurements resolution. Prior to the measurement, the gold electrode was cleaned by immersing in RCA solution as mentioned previously. The crystal holder was cleaned with UV-ozone irradiation for 10 min. Cleaned crystal was used immediately by

immersing into the aqueous solution of 20 mM Sodium 3-mercapto-1-propanesulfonate (MPS) for 2 hr (Hodak et al., 1997). Set the temperature control of the QCM apparatus at room temperature (25^{o}C). The crystal was then mounted on a standard holder and exposed to 200 mL DI water. A schematic diagram of the QCM system is shown in Figure 3.4. When the baseline of resonance frequency was stable for more than 15 min, PDDA solutions were injected into an open chamber at a proper rate using a micropipette to start the process of forming the self-assembled monolayer. The resonance frequency of quartz crystal sensor changes upon adsorption or desorption of molecule on the surface of sensor, which was simultaneously recorded in real time. This change confirmed the interaction between the negatively- and positively-charged layers which indicated an increase of mass adsorption onto the studied surface. The surface was eventually saturated with the PDDA layer. The decrease in frequency for the LbL self-assembly was suggested for the optimum deposition time of PDDA. The same procedure was used for analyzing SF and Col adsorption onto PDDA positive charge surface. (Nawae et al., 2018)

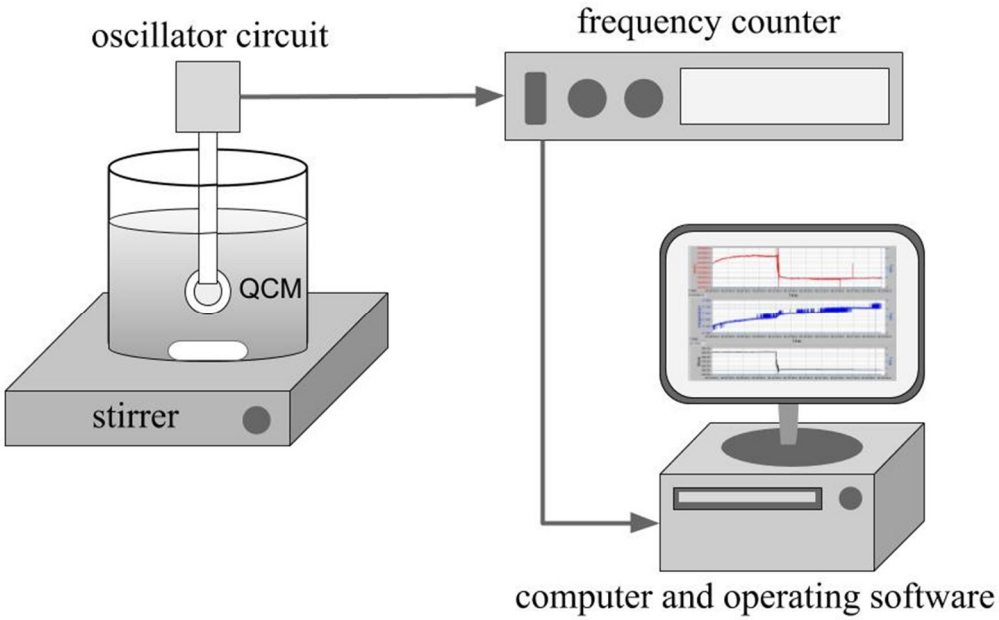

Figure 3.4 Schematic diagram of the QCM system.

3.7 Wettability and Surface Energy Measurement

Polymer wettability is a fundamental surface property that plays a pivotal role in engineering, biomedical, and biomaterials (Awaja et al., 2009). The wettability of a material surface is the tendency of a liquid to spread on a solid substrate and generally analyzed in terms of the contact angle (CA) at the three-phase boundary where a solid, liquid and vapor intersect (Kumar and Prabhu, 2007). Measurement of the water contact angle was performed by the sessile drop method (Taniguchi et al., 2001) using an OCA 15EC instrument (Dataphysics Instruments, Germany). In this test, the volume of the DI water droplets at 1 µl was placed on the multilayer substrate and allowed to spread. The images of a spreading sessile drop are recorded and measured by fitting a circle around the water droplet in contact with the substrate surface and then calculating the angle between the tangent drawn at the triple point between the three phases by the SCA 20 software. Each measurement was repeated at least five times and an average taken.

One of the important applications of the contact angle measurement is the assessment of the surface free energy (SFE) of the solid. The SFE is normally measured indirectly of the contact angle with several liquids. In this study, the Owens, Wendt, Rabel and Kaelble (OWRK) method was used for calculating SFE of $[PDDA/SF/PDDA/Col]_n$ film which considers the geometric mean of the dispersive and polar parts of the liquid's surface tension and of the solid's surface energy (Owens and Wendt, 1969). The selected test liquids were water, formamide, and ethylene glycol. The solid SFE components (i.e. dispersive and polar) of these liquids are provided in Table 3.1.

Table 3.1 Surface tension (SFT) of the test liquids.

Liquid	Surface tension (mN m^{-1})		
	Dispersive, γ_L^d	Polar, γ_L^p	Total, γ_L
Water (Yarce et al., 2016)	19.9	52.2	72.1
Ethylene glycol (Yarce et al., 2016)	29.0	19.0	48.0
Formamide (Gaillard et al., 2016)	34.4	23.5	57.9

This approach divides the surface energy into a polar part $\left(\gamma_S^p\right)$ and a dispersive part (γ_S^d). The combining rule proposed by the OWRK model that can be used to calculate SFE is shown in equation (1).

$$\frac{\gamma_L(1+cos(\theta))}{2\left(\gamma_L^d\right)^{1/2}} = \left(\gamma_S^p\right)^{1/2}\left(\frac{\gamma_L^p}{\gamma_L^d}\right)^{1/2} + \left(\gamma_S^d\right)^{1/2} \quad (1)$$

The resulting equation is a linear equation of the type y = mx+c. Plotting $\frac{\gamma_L(1+cos(\theta))}{2\left(\gamma_L^d\right)^{1/2}}$ vs. $\left(\frac{\gamma_L^p}{\gamma_L^d}\right)^{1/2}$, as shown in Figure 3.5 allows the estimation of the dispersive and polar components of the solid SFE. The slope will be $\left(\gamma_S^p\right)^{1/2}$ and the y-intercept will be $\left(\gamma_S^d\right)^{1/2}$. Finally, the total SFE (γ_s) is determined by the sum of polar and dispersive components ($\gamma_s = \gamma_s^d + \gamma_s^p$).

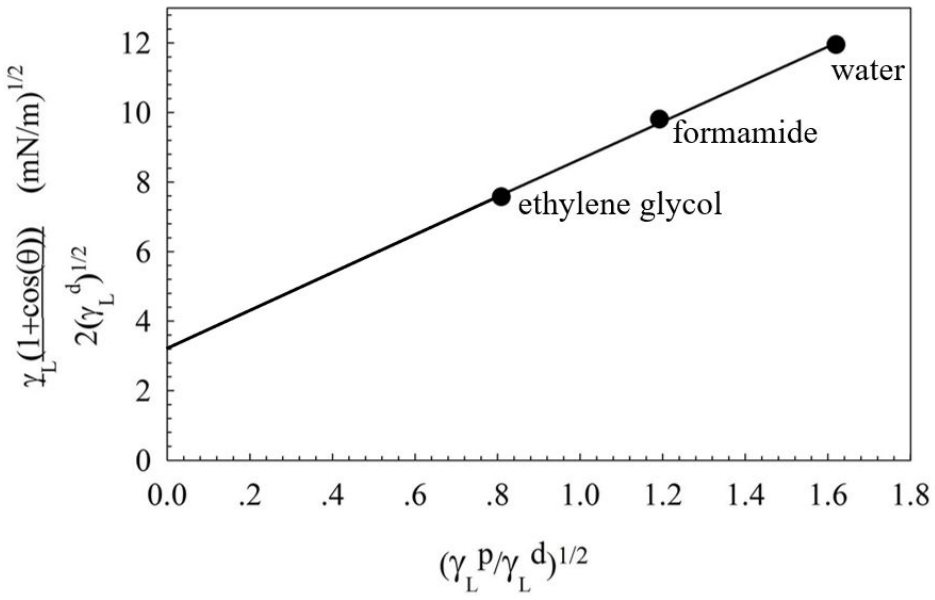

Figure 3.5 Determination of polar and dispersive components of SFE.

3.8 Scanning Electron Microscopy

A Scanning electron microscopy (SEM; Quanta400, FEI, Czech Republic) was used to observe the morphology and characterization of film thickness that verifies by top-view and cross-sectional SEM image, respectively. Firstly, the samples were mounted on aluminum stubs using double-sided adhesive tape and pre-coated with gold using a gold sputter-coating machine (SPI Supplies, Division of Structure Probe. Inc., West Chester, USA). Subsequently, Imaging was performed at beam accelerating voltages from 20- 25 keV. All images were taken from random sites on each sample in order to visualize the general morphological features of $[PDDA/SF/PDDA/Col]_n$ multilayer film.

3.9 Atomic Force Microscopy

The topography of $[PDDA/SF/PDDA/Col]_n$ multilayer film was observed using atomic force microscopy (AFM; Nanosurf EasyScan 2, Liestal, Switzerland) with an ACL-A cantilever (AppNano). A non-contact mode in air was conducted using a silicon tip with an aluminum coating on the reflex side with a radius of 10 nm and a height of 14-16μm. Variations in tip height are recorded while the tip is scanned repeatedly across the sample, producing a topographic image of the surface. AFM topographic images of 20 μm × 20 μm were taken at random positions at a resonance frequency of ~180 kHz. The value of the root mean square (RMS) roughness was analyzed by Gwyddion software, which is an open source software to filter all grains observed in the AFM image and identify grain size distribution. Furthermore, AFM analysis was also used to measure the film thickness by scratching the surface with a thin blade, which penetrates down to the glass substrate and results in accurate thickness measurement. (Nawae et al., 2018)

3.10 Fourier Transform Infrared Spectroscopy

The chemical functional groups of the multilayer film were obtained by Fourier transform infrared (FTIR) spectrometer (Equinox 55, Bruker, Ettlingen,

Germany). The FTIR spectra of samples were recorded in an attenuated total reflection (ATR) mode at a wavenumber range of 400-4000 cm^{-1} and 256 averaging scans at 4 cm^{-1} resolution under ambient conditions.

3.11 Raman Spectroscopy

Raman scattering can explore a material's structure, composition, and condition. This study, Raman spectroscopy was used to investigate layered structures of multilayer film. Microscopic Raman scattering measurements were recorded with a confocal Raman (RAMANforce; Nanophoton, Osaka, Japan) in the Raman shift range of 200-4000 cm^{-1}. The Raman spectra were acquired using a laser excitation of 532 nm and 100x (NA 0.90) microscope objectives.

3.12 Cell Culture

In this study, MC3T3-E1 cells, a mouse calvaria osteoblast-like cell line, were used for cells experiment. The cells were cultured in Alpha-Minimum Essential Medium (α-MEM, Gibco, Invitrogen, USA) with the addition of 10% fetal bovine serum (FBS, Gibco, Invitrogen, USA), 1% penicillin and streptomycin (Gibco, Invitrogen, USA), and 0.1% Fungizone (Gibco, Invitrogen, USA), at 37 °C in a in a humidified 5% CO_2 incubator. The culture medium was replenished every 2-3 days. (Nawae et al., 2018)

3.13 Cell Proliferation

Cell proliferation was evaluated by a nonradioactive, water-soluble tetrazolium salt (WST-1) colorimetric assay (Roche Diagnostics, Germany). The measurements of cell proliferation were performed on days 1, 3, 5, and 7 (Yamamura et al., 2015). The samples were then removed to a fresh well plate. Then, 250 μL of culture medium, combined with 30μL of WST-1, was added to each well and incubated at 37 °C with 5% CO2. After 4 h, the absorbance was measured at 460 nm using an ELISA plate reader. (Nawae et al., 2018)

3.14 Alkaline Phosphatase Activity

An alkaline phosphatase (ALP) activity test was carried out to measure the presence of osteoblast cells along with the formation of new bone. MC3T3-E1 cells were seeded on a well culture plate, with a complete, culture media supplemented with 50 μg/mL of ascorbic acid, 50 mM dexamethasone, and 1M β-glycerophosphate disodium salt hydrate. (Nawae et al., 2018)

The cells were rinsed twice with phosphate buffer solution (PBS) and scraped into 0.2 mL of alkaline lysis buffer (Ji, 2010) after cell culture at days 7, 14, and 21 (Li et al., 2016) in order to cover the cells growth curve (lag phase, log phase, stationary phase and decline phase). Following that, the solution was centrifuged at 12,000RPM at 4 ºC for 10 min. The supernatant was collected and analyzed for ALP activity. The ALP activity was calculated for the molar absorptivity of *p*-nitrophenyl at 405 nm using an alkaline phosphatase assay kit (Abcam®, Cambridge, UK), based on the use of 2-amino-2-methyl-1-propanol buffer. (Nawae et al., 2018)

3.15 Total Protein Assay

Total protein content in the cell lysates was determined using a bicinchoninic acid (BCA) protein assay kit (Pierce, Thermo Scientific, USA), following the manufacturer's instructions. 1% Triton X in PBS was used as solution for cell lysates. The multilayer films were washed twice with 800μL of 1% Triton X in PBS for each well. The cell lysis solution was then added in order to extract the cellular proteins. The samples were alternately frozen at -70 ºC for 1 h, thawed at room temperature for 1 h which was repeated 3 times. After which, the supernatant was removed from the pellet by centrifugation at 12000 rpm for 10 min. (Nawae et al., 2018) The absorbance of these samples was measured at 595 nm on days 7, 14, and 21 (Beloti and Rosa, 2005) in order to cover the cells growth curve. Total protein content (μg/sample) was calculated from a standard curve of absorbance versus known concentrations of bovine serum albumin.

3.16 Nano-indentation Measurement

Elastic modulus was evaluated by using nanoindentation technique through an AFM (Nanosurf Easyscan2, Liestal, Switzerland) and fitting the obtained force-distance curve to Hertz's theory.

A force-distance curve is a graph of interaction forces versus the distance of the AFM tip and the sample surface. To obtain a force-distance curve, the tip is moved perpendicular to the sample surface in Z-direction. After the tip contact to the surface, the bending is occurred. The tip-sample force (F) is described by Hooke's law:

$$F = -k_c \delta_c \tag{2}$$

Where k_c is the spring constant of the cantilever and δ_c is the cantilever deflection. The deflection and the force are considered positive when the cantilever bends away from the sample (repulsive force) and negative when the cantilever bends towards the sample (attractive force).

The distance-controlled in vertical direction during the measurement is not the actual tip-sample distance D, but the distance Z between the sample surface and the rest position of the cantilever (Figure 3.6). For the calculation of the tip-sample distance D, the following equation is used:

$$D = Z - \delta_c \tag{3}$$

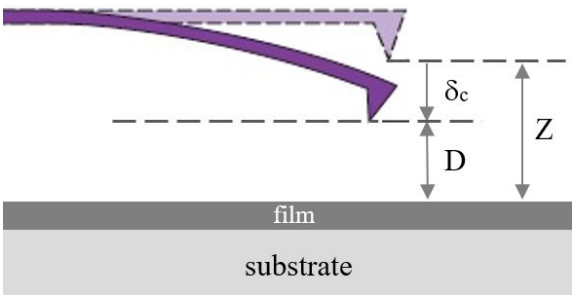

Figure 3.6 Cantilever deflection.

Deflection of the cantilever after the zero line is depended on the interaction between the tip and the sample. During the approach to the surface, an attractive long-range force on the tip bends the cantilever toward the surface. Then the tip suddenly jumps into contact with the surface. After the tip and the sample is completely contact, the characteristic of the curve is depended on the mechanical properties. (Phooplub, 2018: 58)

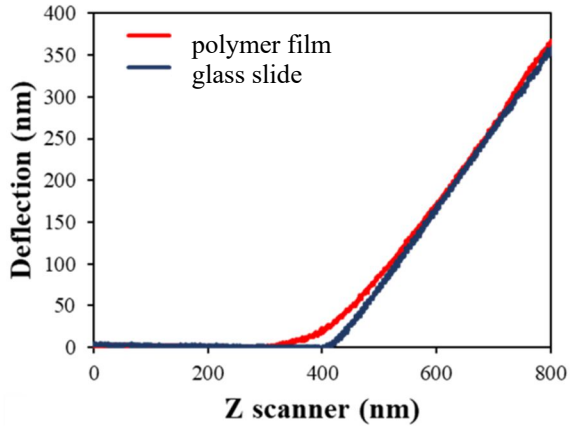

Figure 3.7 The deflection curve of glass slide and polymer. (Phooplub, 2018: 58)

The slope of this regime is depended on the Young's modulus of the materials as shown in Figure 3.7. That is, the higher slope indicates greater Young's modulus. Young's modulus of the sample is calculated by using Hertz contact mechanics theory. Hertz model considers both the tip and the sample as two spheres and only assumes elastic deformation of the materials (Roa et al., 2011). The contact radius (a) according to the theory is given as:

$$a_{Hertz} = \left(\frac{RF}{K}\right)^{1/3} \tag{4}$$

where R is the tip radius and K is the reduced elastic modulus given by

$$\frac{1}{K} = \frac{3}{4}\left(\frac{1-{v_i}^2}{E_i} + \frac{1-v_s^2}{E_s}\right) \tag{5}$$

Where E is Young's modulus, and υ is Poisson ratio. For subscript s and i are the sample and the indenter, respectively. When $E_i << E_s$, the reduced modulus can be approximated in the form (Phooplub et al., 2018):

$$\frac{1}{K} = \frac{3}{4}\left(\frac{1-\upsilon_s^2}{E_s}\right) \quad (6)$$

For very small indentations the contact radius a can be rewritten as $\sqrt{RD}$.

Determination of mechanical properties of multilayer film, such as Young's modulus, is fundamental importance when the films are used for coating of dental implant. This study analyzed Young's modulus of multilayer film by a nano-indentation technique through AFM. The $[PDDA/SF/PDDA/Col]_{50}$ films were immersed in PBS solution at pH 7, which is normal pH of saliva (Nikolopoulou and Tzortzopoulou, 2007), at 37 ^{o}C for 1-30 day.

3.17 Statistical Analysis

Five samples (n = 5) were used for testing. All data were measured and statistically compared by one-way ANOVA followed by Tukey's HDS test (SPSS 16.0 software package) and the results were reported as mean ± standard deviation (SD). (Nawae et al., 2018) Statistical significance was defined as $*p < 0.05$.

CHAPTER 4

RESULTS AND DISCUSSION

This chapter describes an investigation of the physical, chemical, and morphological characteristics of the multilayer surface to determine the activity of biological responses of osteoblast cell.

4.1 Self-assembled Multilayer Formation

In order to ensure the adsorption of polyelectrolyte is completely binding onto the oppositely charged layers. The QCM technique was used to monitor the real-time kinetics of the adsorption process, which is necessary to establish suitability for the assembly condition. This method is based on a vibrating, quartz crystal resonator. The resonance is disturbed by the addition or removal of mass on the sensor surface. The adsorption of the layer was studied until a constant frequency was reached. The typical records of frequency shift (Δf), as a function of adsorption time for PDDA, SF, and Col, are shown in Figure 4.1. The frequency shift decreased rapidly during the initial period, which indicated the adsorption happened rapidly, and intensely at the interface in the first 2-10 min (Nawae et al., 2018). The frequency shift recorded for Col were much higher than SF. For Col adsorbed on PDDA, Δf was about -168 Hz at the fundamental frequency for 20 h; for SF, values of Δf = -149 Hz were measured. It may be noted that the size of these molecules is about 1.5 nm × 300 nm for collagen (Kadler et al., 1996) and 15 nm × 60 nm for SF (Inoue et al., 2000). The adsorption of 10 mM PDDA and 0.1 mg/mL SF self-terminated after 3 and 15 min, respectively. It was assumed that a monolayer had formed onto the surface once the frequency reached a steady state. Whereas the adsorption of 0.1 mg/mL Col was slower and displayed no plateau by itself. The result is similar to S.E. Majd et al. 2014 (Majd et al., 2014).

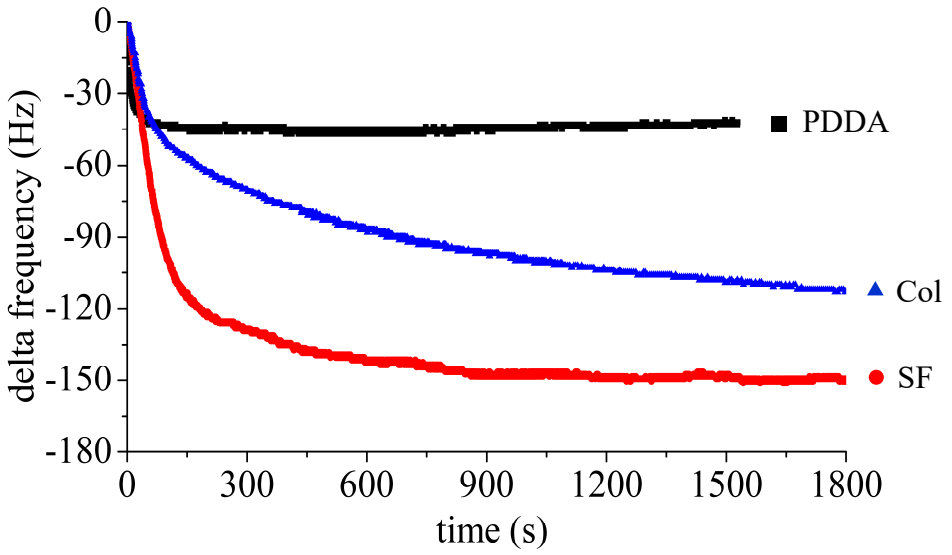

Figure 4.1 Frequency shift and stability for self-assembled layers of PDDA, SF, and Col.

4.2 Topographical and Morphological Observation

In this research, AFM and SEM were used to observe both the topography and surface roughness of LbL self-assembled film. The results of self-assemble multilayer films via negative-positive charge interaction demonstrated the mechanism of the organization as follow: the first layer of positively charged PDDA molecules was deposited on the surface of the substrate. Then, the second layer of negatively charged SF molecules attached themselves to the first layer of PDDA molecules. Later, the third layer of positively charged PDDA molecules deposited themselves onto this second layer of negatively charge SF molecules. Finally, the fourth layer of negatively charged collagen molecules adhered on the third layer of positively charged PDDA molecules (Nawae et al., 2018). The results revealed that the unmodified glass slide (n = 0) exhibits a smooth surface, whereas the LbL-modified surfaces showed granular structures, which were evident from the three-dimensional images (Figure 4.2).

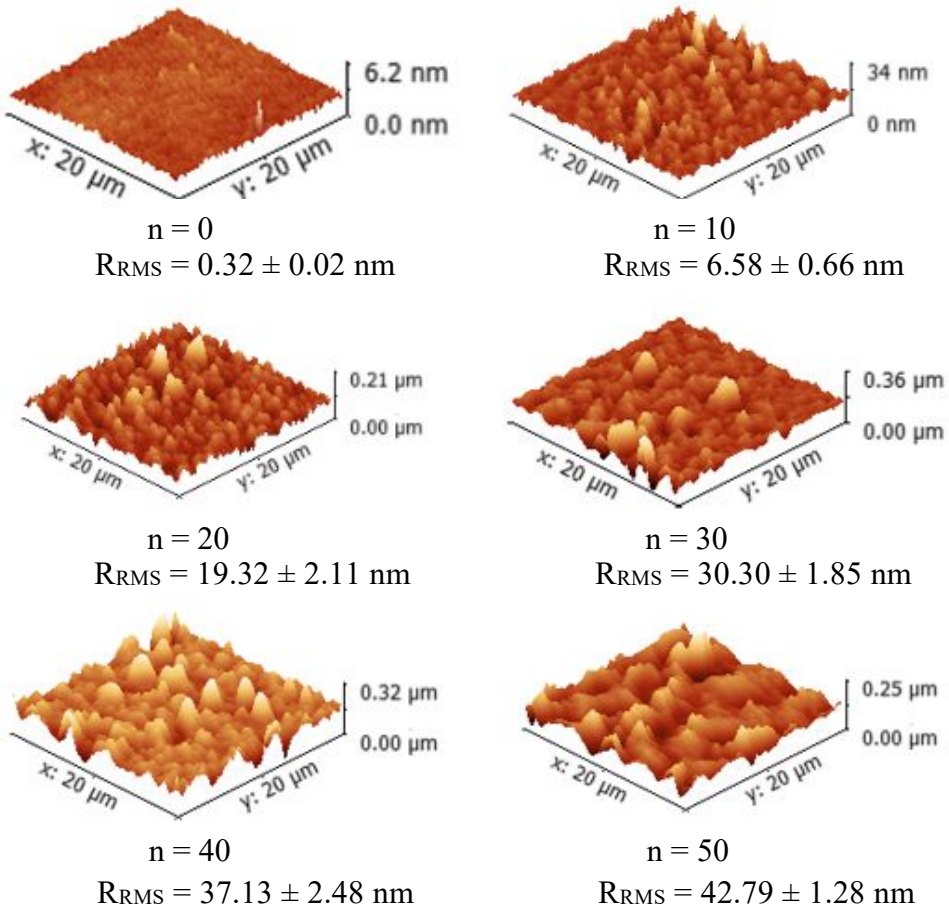

Figure 4.2 Surface topology of [PDDA/SF/PDDA/Col]$_n$ film studied by AFM.

The topography change was further quantified by a roughness measurement expressed in terms of RMS roughness (R_{RMS}), which describe the height of the surface structure. The RMS surface roughness of the multilayer films is shown in Figure 4.3. Before modification, the top view of the glass slide surface appeared to be comparatively smooth (R_{RMS} = 0.32 ± 0.02 nm). After modification, the outermost surface roughness of the multilayer films on the glass substrates increased with increasing number of quad-layers. The results displayed that the morphology of the assembled material become rougher in a range of tens of nanometers. This probably comes from the aggregation of self-assembled PDDA layers, which was beneath the collagen layer. This aggregation layer had the effect of inducing surface roughness. Importantly, the surface roughness has an influence on physical functionality and biological performance. (Nawae et al., 2018)

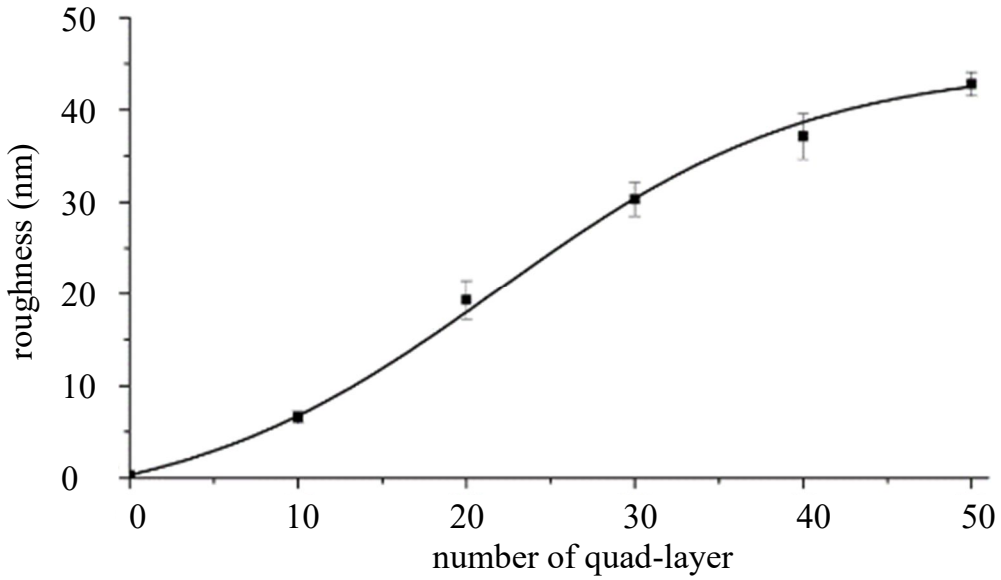

Figure 4.3 Surface roughness values of [PDDA/SF/PDDA/Col]$_n$ film determined from AFM analysis.

A SEM was used to characterize the topography of the multilayer films. The SEM images showed that the collagen could form the parallel fibril structures covering the surface of the SF/PDDA film in characteristically long, bulging, and overlapping patterns (Figure 4.4). The parallel fibril structures might come from the dynamic force line of solution during dipping (Collier et al., 2018). This dynamic force line probably dragged the collagen molecules such that they suddenly deposited themselves into a parallel direction on the surface of the positively charged PDDA layers (Vesentini et al., 2013). Then, the collagen molecules that were deposited in parallel acted as the nucleating points for fibrillation (Muiznieks and Keeley, 2013). There were no differences in the fibril sizes of all samples, which demonstrated that the positively charged PDDA layers of all samples did not affect on the fibril formation of the collagen. As the number of quad-layers increased, the multilayer film showed closely packed collagen fibrils which seemed to be thicker. This result corresponded to the results of the AFM imaging that showed higher than average height. (Nawae et al., 2018)

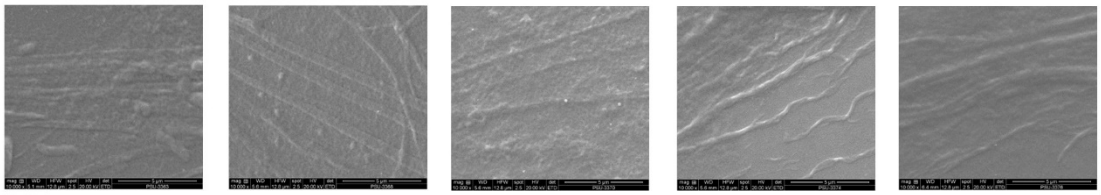

Figure 4.4 SEM images (10,000x) demonstrating the surface of [PDDA/SF/PDDA/Col]$_n$ film after LbL deposition.

The thickness of the [PDDA/SF/PDDA/Col]$_n$ film was calculated by AFM and cross-sectional SEM image and the results by AFM are shown in Figure 4.5. The [PDDA/SF/PDDA/Col]$_n$ deposition was nano-sized, and the thickness of the deposition increased approximately 7 nm in each quad-layer. Figure 4.6 demonstrates a typical cross-sectional SEM image of the glass substrate coated with 10, 20, 30, 40, and 50 quad-layers. The thicknesses of the coatings on the substrate were evaluated by Image J software. The results were nearly the same as the AFM method. The thickness of the fabricated film showed that growth increased with the number of *n*. (Nawae et al., 2018)

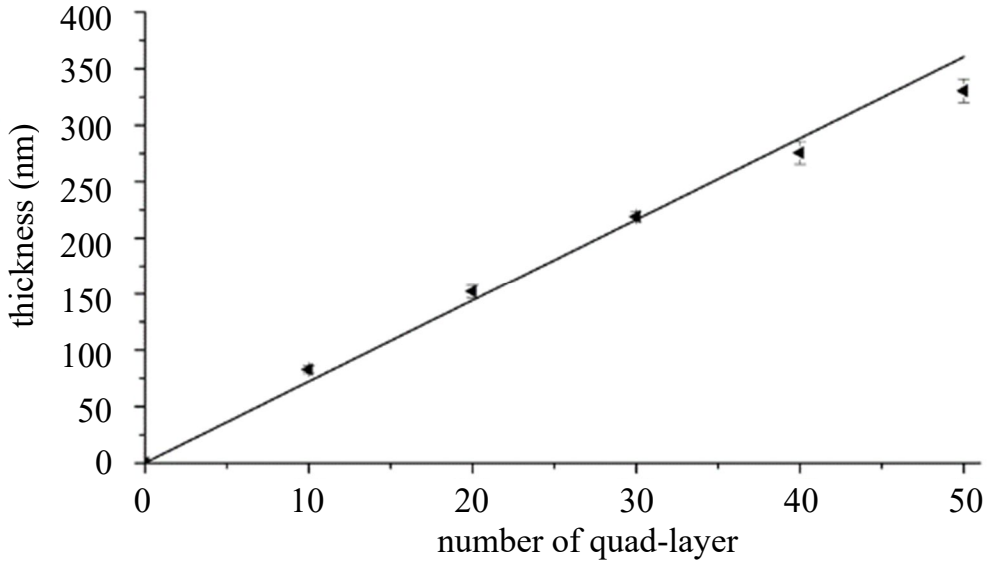

Figure 4.5 Thickness of the self-assembled [PDDA/SF/PDDA/Col]$_n$ multilayer films evaluated by AFM.

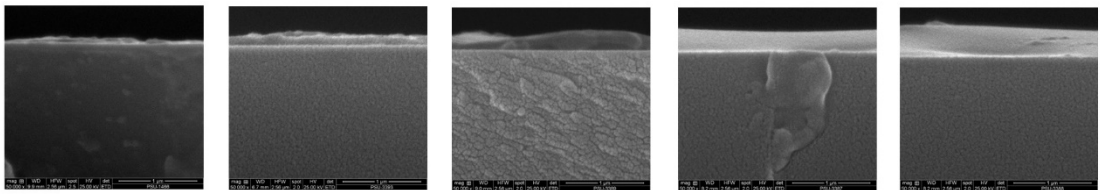

n = 10 n = 20 n = 30 n = 40 n = 50

Figure 4.6 Cross-sectional SEM image (50,000x) of [PDDA/SF/PDDA/Col]$_n$ film.

4.3 Wetting Properties of the LbL Self-assembled Films

The wettability and SFE were selected to evaluate the performance of LbL self-assembled films. Wettability studies usually involve the measurements of CA, which indicates the degree of wetting when a solid and liquid interact. To investigate the mechanism by which the PDDA/SF/PDDA/Col molecules were deposited onto the substrates under the different number of quad-layer conditions, which resulted in almost no difference on surface wettability. After fabrication of the multilayer film, the water contact angle did not show fluctuation (Figure 4.7). This constant water contact angle possibly indicated that it does not depend on a growing coating density from 10 to 50 quad-layers (Nawae et al., 2018). A hydrophilic glass slide (CA = 21.0 ± 1.2°) was obtained by the formation of the hydroxyl group on the RCA-cleaned surface. The patterned multilayer surface with nanostructure displayed a significantly decreased surface hydrophilicity; i.e., increase in water contact angle. A low contact angle (CA<90°) of multilayer films (CA ≈ 63.8-66.4 ± 1.0°) corresponds to high wettability, and the fluid will spread over a large area of the surface. If the contact angle is greater than 90°, it corresponds to low wettability, and the fluid will minimize contact with the surface and form a compact liquid droplet while high contact angle value (CA>150°) shows poor spreading which indicates minimal contact between the liquid droplet and the surface and corresponds to a superhydrophobic behavior. It revealed that the hydrophilicity of [PDDA/SF/PDDA/Col]$_n$ film was influenced by their outer surface morphology. Furthermore, the liquid contact angle measurements can be used to determine the surface energy of a material.

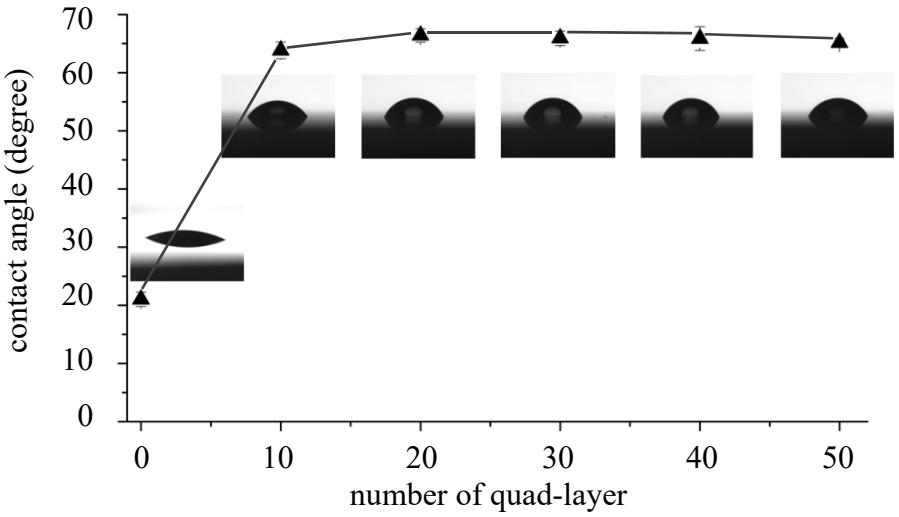

Figure 4.7 Water contact angle of [PDDA/SF/PDDA/Col]$_n$ film.

From Equation (1), the contact angle value was applied to determine the dispersive and polar components of the surface energy. A graphical representation of the OWRK method for the glass and multilayer surfaces is shown in Figure 4.8. The slope of the graph gives the polar component and the vertical intercept gives the dispersive component of the solid SFE (Nawae et al., 2018). The total SFE of the solid is the sum of the two parts and the results are shown in Figure 4.9.

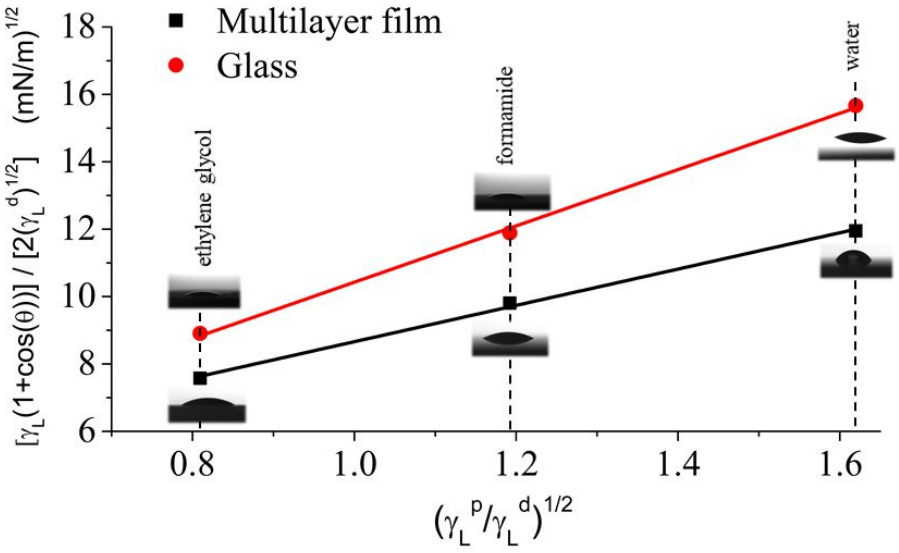

Figure 4.8 Representative SFE calculation graph based on the OWRK model. for glass and multilayer film.

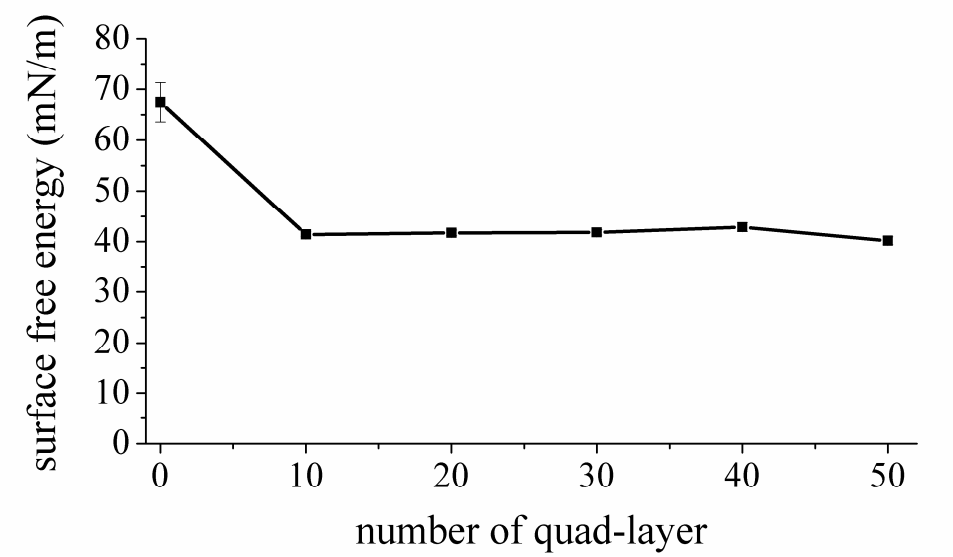

Figure 4.9 Surface free energy of [PDDA/SF/PDDA/Col]$_n$ film.

Figure 4.9 shows changes in the apparent surface free energy of a multilayer solid surface calculated from Eq.1 as a function of the contact angle using three different liquids. The SFE decreased initially compared with a cleaned glass slide while the SFE for the [PDDA/SF/PDDA/Col]$_n$ film was constant at approximately 42 mN/m with increasing *n*. The modification step of the [PDDA/SF]$_n$ film was characterized as a lower SFE than the [PDDA/Col]$_n$ film (≈ 37 and 44 mN/m, respectively). The difference in SFE indicated a dominance of either SF or Col in the outermost layer after the corresponding coating step. (Nawae et al., 2018)

The contact angle and SFE of the LbL self-assembled films were about 65^o and 42 mN/m, respectively, while the contact angle and SFE of pure collagen film was about 110^o and 68 mN/m (Taraballi et al., 2013). This low contact angle and SFE of LbL self-assembled films possibly came from specific topographical structures which showed hydrophilic characteristics. Notably, there were no differences in the contact angles of all samples of LbL self-assembled films. This result might indicate that the high outermost surface roughness, which generally effected on inducing wettability, was disturbed by the molecular mobility of the films with different thicknesses (Sultana et al., 2008; Mazur et al., 2011). The films of greater thickness possibly showed unique molecular mobility, which affected on the wettability which

reduced the high outermost surface roughness (Kubiak et al., 2011). The surface roughness, wettability, and different thicknesses, which have different molecular mobility, possibly resulted in interference in the biological performance of these LbL films. Overall, the relatively stable contact angle and SFE when depositing the PDDA/SF/PDDA/Col indicated that the LbL self-assembly had good hydrophilicity. (Nawae et al., 2018)

4.4 Fourier Transform Infrared Spectroscopy Characterization

The molecular organization of LbL self-assembled films was characterized by FTIR and Raman spectroscopy. Wavenumbers of infrared (IR) spectroscopy are associated with the characteristics of chemical functional groups in multilayer films. The different wavenumbers of chemical functional groups are related to the structural changes in the multilayer films that were determined by FTIR (Figure 4.10). All samples showed peaks at around 800-900 cm^{-1} which represented the Si-O-Si groups (Jang et al., 2015). Peaks at around 700 cm^{-1} indicated the Si-C groups for all samples (Jana et al., 2013). The LbL multilayer films showed peaks at around 1624 and 1530 cm^{-1} which were the amide I and amide II (Ghaeli et al., 2017). The results showed no peaks of amide I for n = 10. On the other hand, the LbL self-assembled films of n = 20, 30, 40, and 50 displayed amide I vibration, especially n = 50 which had the highest wavenumber of amide I at around 1634.27 cm^{-1}. This indicated that the higher layers of LbL self-assembled films showed more molecular movement than the others (Nawae et al., 2018). The amide II displayed fluctuation of the peaks at 1530.32, 1530.32, 1539.32, and 1530.32 cm^{-1} of n = 20, 30, 40, and 50, respectively and no peaks of amide II for n = 10.

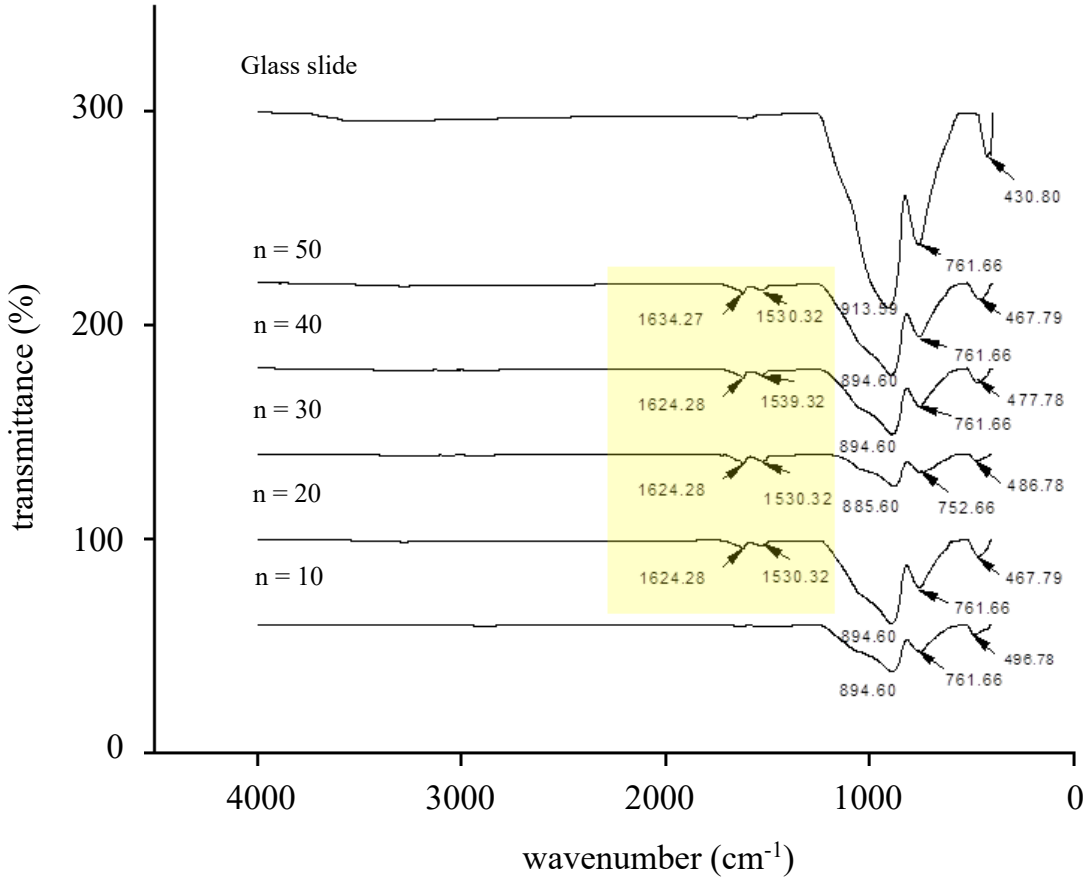

Figure 4.10 FTIR spectra of $[PDDA/SF/PDDA/Col]_n$ film.

4.5 Raman Spectroscopy

The Raman spectra of samples are presented in Figure 4.11. The glass slide showed Raman shifts in the high-frequency range at around 1547.76, 1374.94, and 1096.84 cm^{-1} which were identified as different O-Si vibrations (Osipov et al., 2015). On the other hand, 780.99 and 557.97 cm^{-1} exhibited in the low-frequency range indicated stretching and bending of Si-O-Si (Osipov et al., 2015). LbL multilayer films displayed the chemical functional groups in the high and low-frequency range of Raman shifts. The Raman shift of the LbL multilayer films at 1661.48 cm^{-1} is amide I (Téllez S, 2017). LbL multilayer films of n = 20, 30, 40, and 50 had Raman shifts of amide III at 1429.59, 1438.03, 1447.47, and 1434.03 cm^{-1}, respectively (Kessler et al., 2015). The LbL self-assembled films of n = 10 showed no amide I or amide III which

was similar to the glass slide. This possibly came from the very thin film of n = 10 that did not show the Raman spectrum. In contrast, n = 20 to n = 50 which had sufficient thickness led to the amide I and amide III peaks and also found that the thicker film had a higher Raman shift than the thinner film. This revealed that the thick films had more molecular mobility of amide I and amide III than the thin LbL self-assembled films. This might have an effect on the physical functionality which can be related to biological performance (Nawae et al., 2018). Furthermore, the result demonstrated that the Raman shifts at 1261.22 and 1231.89 cm^{-1} of n = 50 represent molecular skeletal stretching (Talari et al., 2015).

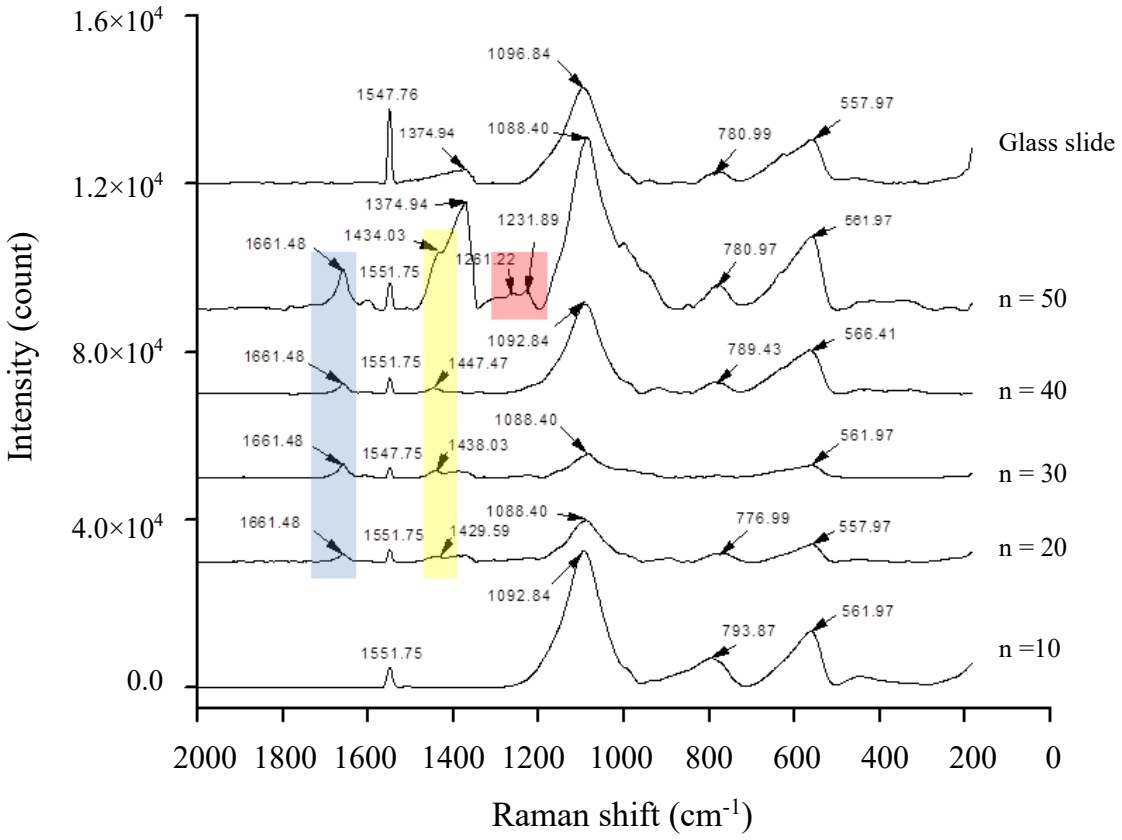

Figure 4.11 Raman spectra of [PDDA/SF/PDDA/Col]$_n$ films.

4.6 Cell Proliferation on LbL Self-assembled Films

In this study, the biological performance of osteoblast-like MC3T3-E1 cells on LbL self-assembled films was evaluated with cell proliferation, ALP activity, and total protein absorption. The WST-1 assays of cell proliferation on the multilayer films are presented in Figure 4.12. The results showed that the substrate with LbL self-assembled films was able to induce cell proliferation, particularly with a greater number of layers. This was related to the high surface roughness of those layers. Cell proliferation was the biomarker to indicate the potential of the LbL self-assembled films to act as a nucleating surface for osseointegration. The proliferation of MC3T3-E1 cells steadily increased in each group of multilayer films from day 1 to day 5 due to the proliferation kinetics of the osteoblasts, and then decreased on day 7 of the cell culture. In all groups of the multilayer films (including the control), cell proliferation increased on day 5, which indicated that the MC3T3-E1 cells adhered as well as proliferated in all groups. However, in the 40 quad-layer films on day 5, a tendency towards the highest proliferation was demonstrated. (Nawae et al., 2018)

Furthermore, the results showed that the substrate with the LbL self-assembled films had higher cell proliferation than the substrate without the LbL self-assembled films. This indicated that the collagen outermost layer had a suitable roughness coupled with the characteristics to enhance cell proliferation. Interestingly, previous research demonstrated that the substrate with high surface roughness and hydrophilicity showed the ability to induce cell proliferation (Wang et al., 2016; Zareidoost et al., 2013). Furthermore, the molecular characteristics of collagen, which has an amino acid sequence of RGD, could induce cell proliferation (Ao, 2017). Interestingly, previous research also demonstrated that the outermost layer showed suitable mobility which led to the organization of a structured surface. The organized, structural surfaces had a certain molecular conformation, which had the effect of promoting cell adhesion (Sinani et al., 2003), which in turn led to enhanced cell proliferation (Gong et al., 2007). Notably, n = 30 of the LbL film showed unique cell proliferation, which might have arisen from the suitable mobility of that layer which was also possibly related to certain, structural arrangements of the collagen molecule on the outermost surface (Huang et al., 2015). This suitable, structural arrangement

might show regular conformation, which again has an effect on enhancing cell proliferation (Zhao et al., 2014). Notably, the results displayed that all samples had the highest cell proliferation at day 5 and then decreased at day 7. This comes from the effect of confluence on decreasing cell proliferation for all samples (Blacklocka et al., 2011; Pavel et al., 2018). Remarkably, cells still lived on samples after day 7. This was confirmed by expression of ALP activity and total protein absorption which gradually increased from day 7 to 21. The increasing of that expression refers to the live status of cells (Wang et al., 2017).

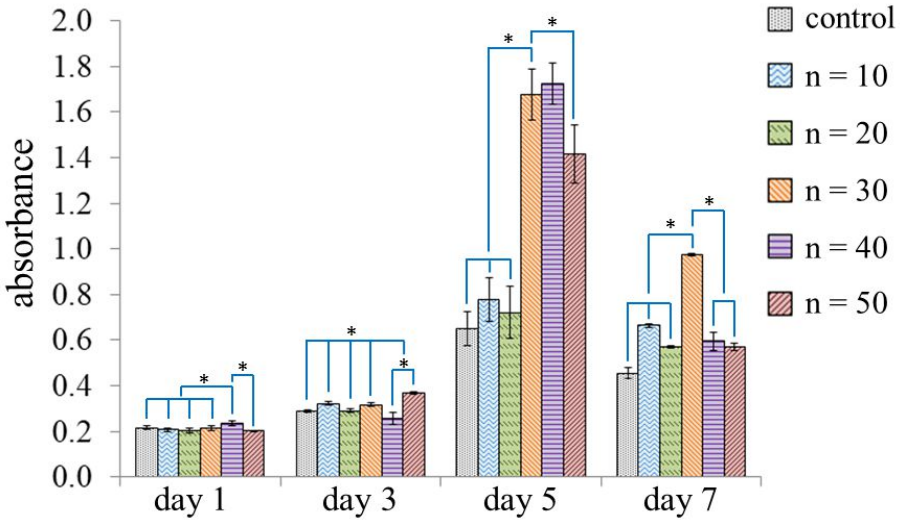

Figure 4.12 WST-1 assay of MC3T3-E1 cells grown on $[PDDA/SF/PDDA/Col]_n$ film at days 1, 3, 5, and 7. The symbol (*) represents significant changes in cell proliferation of MC3T3-E1 cells ($p < 0.05$).

4.7 Alkaline Phosphatase Activity on LbL Self-assembled Films

For ALP activity, it is related to the early stages of bone formation and is a biomarker. In this research, ALP activity indicated the biological ability of the LbL self-assembled films to act as a nucleating surface for osseointegration. Figure 4.13 shows the ALP activity of MC3T3-E1 cells seeded on multilayer films at days 7, 14, and 21 of the cell culture. The results showed that all multilayer films supported MC3T3-E1 cell differentiation. ALP activity in the MC3T3-E1 cells for each group

gradually increased with the culturing time from days 7 to 21 and was found to be at its highest on day 21. Furthermore, ALP activity at days 7 and 14 was significantly higher on the 50 quad-layer films compared to the other groups which showed similar ALP values with no significant difference. This indicated that the surface roughness and mobility might be the main clue for enhancement of ALP activity (Rosa and Beloti, 2003). On the other hand, at around day 21 there were no significant differences in ALP activity. This indicated that the surface roughness and mobility had no effect on ALP activity. This was possibly the cause of the disordered, structural surface, which comes from its erosion and degradation that had an effect on ALP activity. (Nawae et al., 2018)

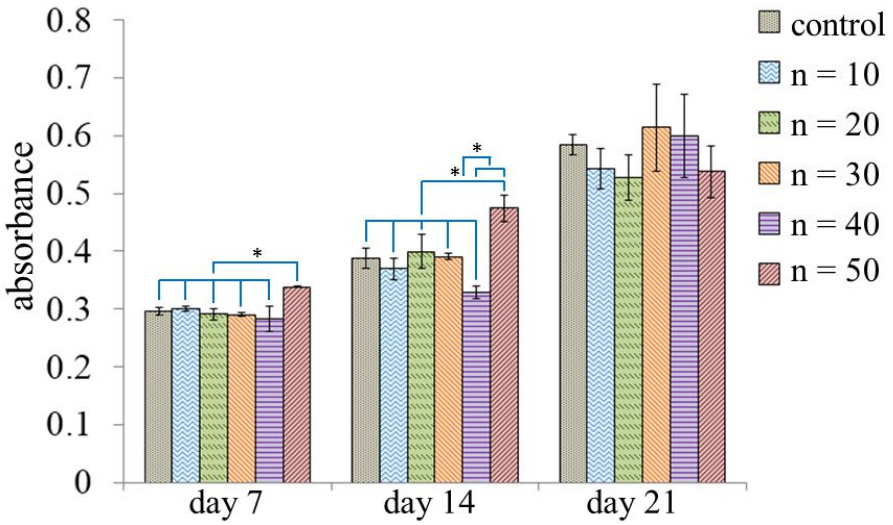

Figure 4.13 ALP activity of MC3T3-E1 cells cultured on $[PDDA/SF/PDDA/Col]_n$ film at days 7, 14, and 21. The symbol (*) represents significant changes in ALP activity of MC3T3-E1 cells ($p < 0.05$).

4.8 Total Protein on LbL Self-assembled Films

Protein synthesis is a very sensitive indicator of cell growth along with proliferation, evaluated by the total protein content. The total protein secreted by osteoblasts during cell culture was determined by BCA analysis on days 7, 14, and 21. The results are displayed in Figure 4.14. It showed that the bio functionalities of collagen on the outer surface could synergize protein. On day 7, the 40 quad-layer film

was similar to that of the 50 quad-layer films, and both showed higher total protein content than the other groups. This might arise from the surface roughness and mobility of those layers. At the early stage of day 7, the surface roughness was probably the clue to induce total protein which adhered to the surface (Rosa and Beloti, 2003) (Deng et al., 2015). For the intermediate stage of day 14, there were no significant differences in total protein for all samples of LbL self-assembled films. This might be the cause of mobility of the outermost layers, which disturbed the protein adhesion (De, 2015). Finally, the total protein of the greater number of layers of LbL films re-approached a high level on day 21. This was because of the mobility which might be the cause of the rearrangement of the outermost layer (Michel et al., 2012). The rearrangement led to a regular, structural organization, which in turn could enhance protein adhesion. This had the effect of increasing the total protein (Zhao et al., 2014).

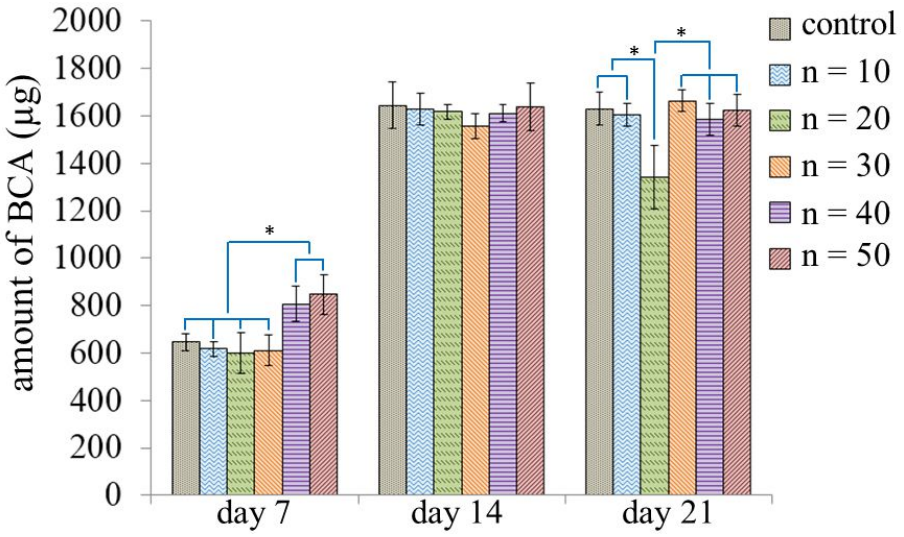

Figure 4.14 Total protein content of MC3T3-E1 cells on $[PDDA/SF/PDDA/Col]_n$ film. The symbol (*) represents significant changes in protein activity of MC3T3-E1 cells ($p < 0.05$).

Eventually, the biological performance of LbL films demonstrated that the surface roughness and molecular mobility were the trigger clues that affected the enhancement of cell proliferation, ALP activity, and total protein which can lead to the promotion of bone formation. (Nawae et al., 2018)

4.9 Mechanical Properties

AFM with a given value of spring constant was taken and was used for the force analysis. Experimentally obtained a force-distance curve for multilayer film on glass slide substrate is explained in Figure 4.15. The curve for loading and unloading is shown by two different lines. The loading curve indicated the deflection while the unloading was obtained during withdrawal processes. It appears that the loading and the unloading curves are not completely overlapped.

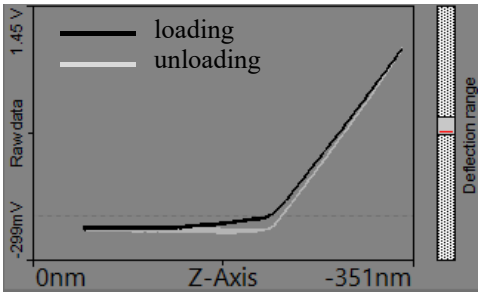

Figure 4.15 Typical mechanical curves obtained by AFM indentation.

Temperature-dependent measurements of Young's modulus were performed on the $[PDDA/SF/PDDA/Col]_{50}$ film in a temperature range from 23 to 37 °C by the use of a thermal stage with a temperature sensor (TMP36, Analog Device, USA) directly glued on the sample. Before measurement, the sample on thermal stage was thermally kept at a constant temperature for an hour. The temperature increments no significantly affected on Young's modulus of the $[PDDA/SF/PDDA/Col]_{50}$ film as shown in Figure 4.16. The value of Young's modulus was slightly fluctuation for temperature between 23 to 37 ºC. This indicated that the silk fibroin could be used for improved collagen film due to its mechanical property. Thus, the combination of silk fibroin and collagen by LbL assembly technique keep the collagen elastic, which is beneficial for dental implant application.

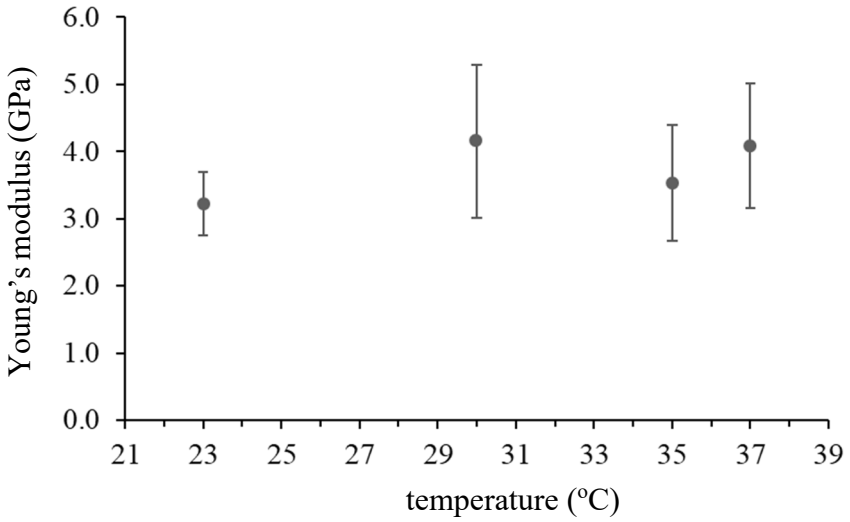

Figure 4.16 A relationship between Young's modulus of [PDDA/SF/PDDA/Col]$_{50}$ film to ambient temperature arisen from 23 ºC to 37 ºC.

Measurement of degradation of the [PDDA/SF/PDDA/Col]$_{50}$ film was performed by incubating in PBS solution pH 7, at 37°C for 30 days. Changes in Young's modulus of the films were measured using a method of nanoindentation by AFM (Figure 4.17). During the early five days of films degradation, Young's modulus decreased due to the relatively fast degradation of the amorphous areas. Young's modulus decreased significantly in early 5 days due to the relatively fast degradation and dissolution of the amorphous polymer components. Thus, the decrease in film stiffness has a favorable effect on cells adhesion according to the result of MC3T3-E1 cells proliferation. After 5 days of the experiment, Young's modulus of the film has fluctuation. This indicated that the process of crystallization of amorphous components has occurred. Overall, polymer degradation plays an important role in the decrease in mechanical properties.

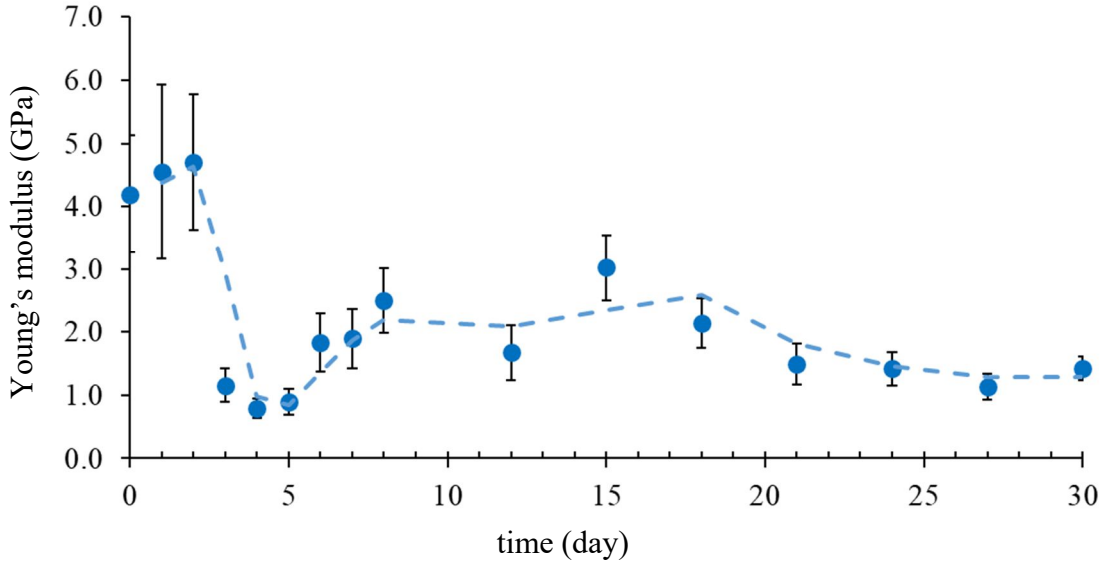

Figure 4.17 The change in Young's modulus of [PDDA/SF/PDDA/Col]$_{50}$ film.

4.10 Practical Use

The goal of modern dentistry is to preserve the teeth for a lifetime. Loss of teeth shows an impact not only on appearance but also on overall health. Dental implants will replace both lost natural teeth and their roots. Among various dental implant materials, Ti and its alloys have been widely used in dental implants due to its chemical stability, biocompatibility and excellent mechanical properties such as low specific weight, high strength to weight ratio, low modulus of elasticity and very high corrosion resistance.

In this research, the results are reported in a preliminary survey of multilayer film on a glass slide substrate, which may not be ideal for application on dental implant. However, as there is virtually no restriction in the choice of the substrate for LbL assembly, this research tested assembly of multilayer film on glass slide substrate because the wetting property of a glass slide and Ti surface after RCA cleaning are no different in surface free energy and contact angle (Figure 4.18).

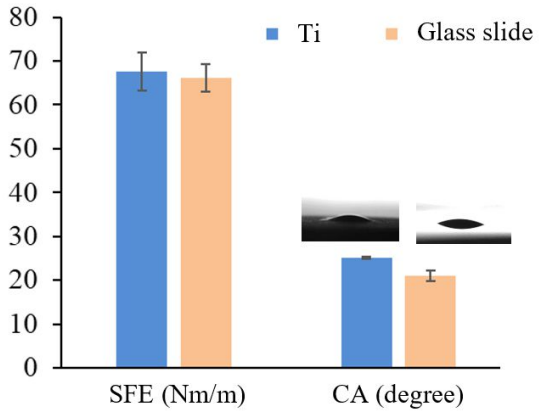

Figure 4.18 Surface free energy and water contact angle of titanium surface.

Comparison of surface roughness, Ti substrate appeared to be comparatively rougher than glass slide substrate. The result displayed that the morphology of the titanium surface becomes rougher in a range of hundreds of nanometers (Figure 4.19). Thus, the surface morphology of multilayer films coat on Ti substrate may differ from the used of glass slide substrate.

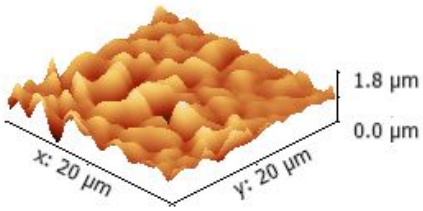

$R_{RMS} = 0.46 \pm 0.11$ µm

Figure 4.19 The AFM surface topology image of titanium.

Figure 4.20 shows the titanium surface morphology coated with SF, PDDA and Col by LbL self-assembly technique. The assemble multilayer films have a homogeneous surface.

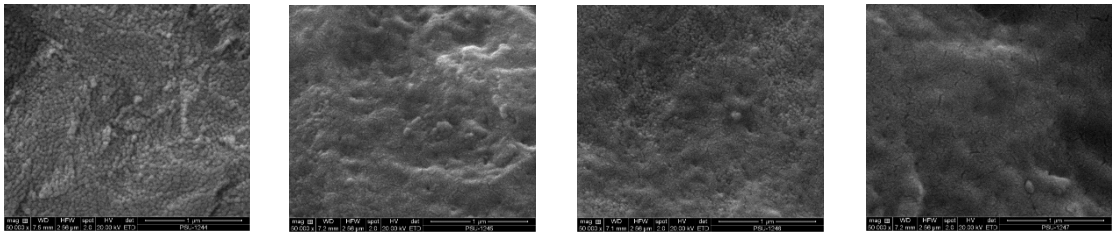

n = 10 n = 20 n = 30 n = 40

Figure 4.20 The surface morphological SEM image (50,000x) of $[PDDA/SF/PDDA/Col]_n$ film on titanium substrate.

CHAPTER 5

CONCLUSIONS AND FUTURES WORK

5.1 Conclusions

The dental implants exhibited significant variations in the surface properties in terms of both structural and chemical composition. The surface modifications of the dental implant material sought to achieve an enhanced biological response. In this research, thin films of SF, Col, and PDDA were fabricated using the LbL self-assembly technique. These thin films were proposed as a nucleating surface for osseointegration in the design of coated dental implant materials. The results indicate that LbL self-assembled films had a rough surface and hydrophilic characteristics. In addition, the surface roughness can be tailored by modifying the number of quad-layers. Importantly, the LbL self-assembled films had a high number of quad-layers and their surfaces showed molecular mobility, which resulted in enhanced biological performance, osteoblast cell proliferation, ALP activity, and total protein absorption. The results indicate that LbL self-assembled films have suitable biological performance as a nucleating surface for osseointegration and are subsequently promising for the design of coated dental implant materials as a foundation for further clinical applications. The LbL technique may therefore be applied to the manufacture of medical devices with advanced functionality on the basis of the improved release of sensitive biologically active molecules.

5.2 Future Works

The results above suggest that osseointegration improvements can be made by coating the implant surface with $[PDDA/SF/PDDA/Col]_n$ multilayer film. This is particularly useful to reduce the duration required for osseointegration since biomaterial scaffolds have shown tremendous promise for early cell attachment.

Hydroxyapatite, the main inorganic component in mammalian bones and teeth, has garnered attention as a surface-coating compound due to its high

osteoconductivity. Nonetheless, some studies have found that hydroxyapatite alone is insufficient during bone formation(Agarwala and Bhagwat, 2005). Further studies may therefore combine HA with [PDDA/SF/PDDA/Col]$_n$ multilayer film to enhance the bone integration speed.

REFERENCES

Agarwala, S. and Bhagwat, A. 2005. Hydroxyapatite as a bone graft substitute: Use in cortical and cancellous bone. Indian J Orthop. 39: 254–256.

Ahn, M., Hwang, I., Jung, C. and Choi, J. 2011. Fabrication of Poly (diallyldimethylammonium chloride) - Patterned Substrates for Patterning of Single Strand DNA Using Ion Implantation. 5: 243–247.

Ai, H., Jones, S.A. and Lvov, Y.M. 2003. Biomedical applications of electrostatic layer-by-layer nano-assembly of polymers, enzymes, and nanoparticles. Cell Biochem. Biophys. 39: 23–43.

Albrektsson, T. and Jacobsson, M. 1987. Bone-metal interface in osseointegration. J. Prosthet. Dent. 57: 597–607.

Alla, R.K., Ginjupalli, K., Upadhya, N., Shammas, M., Krishna, R. and Sekhar, R. 2011. Surface Roughness of Implants : A Review. Trends Biomater. Artif. Organs, 25: 112–118.

Amini, A.R., Laurencin, C.T. and Nukavarapu, S.P. 2013. Bone Tissue Engineering: Recent Advances and Challenges Ami. Crit Rev Biomed Eng. 40: 363–408.

Ao, H. 2017. The synergistic effect of type I collagen and hyaluronic acid on the biological properties of Col/HA-multilayer-modified titanium coatings: an in vitro and in vivo study. RSC Adv. 7: 25828–25837.

Ariga, K., Ji, Q. and P. Hill, J. 2010. Enzyme-Encapsulated Layer-by-Layer Assemblies: Current Status and Challenges Toward Ultimate Nanodevices. Adv. Polym. Sci. 229: 51–87.

Awaja, F., Gilbert, M., Kelly, G., Fox, B. and Pigram, P.J. 2009. Adhesion of polymers. Prog. Polym. Sci. 34: 948–968.

Beloti, M.M. and Rosa, A.L. 2005. Osteoblast Differentiation of Human Bone Marrow Cells Under Continuous and Discontinuous Treatment with Dexamethasone. Braz Dent J. 16: 156–161.

Bernhardt, R., Kuhlisch, E., Schulz, M.C., Eckelt, U. and Stadlinger, B. 2012. Comparison of bone-implant contact and bone-implant volume between 2D-histological sections and 3D-SRμCT slices. Eur. Cells Mater. 23: 237–248.

Blackledge, T.A. and Agnarsson, I. 2010. Bioprospecting Finds the Toughest Biological Material: Extraordinary Silk from a Giant Riverine Orb Spider. PLoS One 5.

Blacklocka, J., Vetter, A., Lankenau, A., Oupický, D. and Möhwalda, H. 2011. Tuning the mechanical properties of bioreducible multilayer films for improved cell adhesion and transfection activity. Biomaterials. 31: 7167–7174.

Boschetti, F., Tomei, A.A., Turri, S., Swartz, M.A. and Levi, M. 2008. Design, Fabrication, and Design, fabrication, and characterization of a Composite Scaffold for Bone Tissue Engineering. Int. J. Artif. Organs. 31: 697–707.

Bosco, R., Beucken, J. Van Den, Leeuwenburgh, S. and Jansen, J. 2012. Surface Engineering for Bone Implants: A Trend from Passive to Active Surfaces. Coatings. 2: 95–119.

Castells-sala, C. and Recha, L. 2013. Current Applications of Tissue Engineering in Biomedicine. J. Biochips Tissue Chips s2.

Collier, T.A., Nash, A., Birch, H.L. and de Leeuw, N.H. 2018. Relative orientation of collagen molecules within a fibril: a homology model for homo sapiens type I collagen. J. Biomol. Struct. Dyn. 1102: 1–13.

Dahiya, V., Shukla, P. and Gupta, S. 2014. Surface topography of dental implants: A review. J. Dent. Implant. 4: 66–71.

Dang, M., Saunders, L., Niu, X., Fan, Y. and Ma, P.X. 2018. Biomimetic delivery of signals for bone tissue engineering. Bone Res. 6.

De, R. 2015. Biological characterization of implant surfaces - in vitro study. Rev Odontol UNESP. 44: 195-199.

Deng, Y., Liu, X., Xu, A., Wang, L., Luo, Z., Zheng, Y., Deng, F., Wei, J., Tang, Z. and Wei, S. 2015. Effect of surface roughness on osteogenesis in vitro and osseointegration in vivo of carbon fiber-reinforced polyetheretherketone-nanohydroxyapatite composite. Int. J. Nanomedicine. 10: 1425–1447.

Elahi, M.F., Guan, G. and Wang, L., 2014. Hemocompatibility of surface modified silk fibroin materials: A review. Rev. Adv. Mater. Sci. 38: 148-159.

Eldo, K. and Sunitha, R.P., 2015. Dental Implant Surfaces : An Overview. Int. J. Clin. Implant Dent. 1: 14–22.

Farokhi, M., Mottaghitalab, F., Samani, S., Shokrgozar, M.A., Kundu, S.C., Reis, R.L., Fatahi, Y. and Kaplan, D.L. 2018. Silk fibroin/hydroxyapatite composites for bone tissue engineering. Biotechnol. Adv. 36: 68–91.

Feldman, D. 2018. Tissue engineering as an example of the need for interdisciplinary fields like. J. Biomed. Imaging Bioeng. 2: 1–2.

Fergal, O.J. 2011. Biomaterials & scaffolds for tissue engineering. Mater. Today. 14: 88–95.

Ferreira, A.M., Gentile, P., Chiono, V. and Ciardelli, G. 2012. Collagen for bone tissue regeneration. Acta Biomater. 8: 3191–3200.

Ficai, A., Andronescu, E., Trandafir, V., Ghitulica, C. and Voicu, G. 2010. Collagen/hydroxyapatite composite obtained by electric field orientation. Mater. Lett. 64: 541–544.

Florencio-silva, R., Rodrigues, G., Sasso-cerri, E., Simões, M.J., Cerri, P.S. and Cells, B. 2015. Biology of Bone Tissue: Structure, Function, and Factors That Influence Bone Cells. Biomed Res. Int. 2015: 1–17.

Frank, R., Rolando, A.G., Lutz, S., Abraham, M., Barbara, D.B., Zvi, S. and Jürgen, G. 2015. A Review on the Wettability of Dental Implant Surfaces: Theoretical and Experimental Aspects. Acta Biomater. 10: 2894–2906.

Frantz, C., Stewart, K.M., Weaver, V.M., Frantz, C., Stewart, K.M. and Weaver, V.M. 2010. The extracellular matrix at a glance. J. Cell Sci. 2010: 4195–4200.

Gaillard, W.R., Waddell, E. and Williams, J.D. 2016. Surface Free Energy Determination of APEX Photosensitive Glass. Micromachines. 7: 1–11.

Gelse, K., Pöschl, E. and Aigner, T. 2003. Collagens - Structure, function, and biosynthesis. Adv. Drug Deliv. Rev. 55: 1531–1546.

Gentile, P., Carmagnola, I., Nardo, T. and Chiono, V. 2015. Layer-by-layer assembly for biomedical applications in the last decade. Nanotechnology. 26: 1-21.

Gero, D., Joseph, M., Jurgen, R. and Ulrich, S. 1991. High1y -Ordered Ultra thin LC Multilayer Films on Solid Substrates. Adv. Mater. 3: 617–619.

Ghaeli, I., De Moraes, M.A., Beppu, M.M., Lewandowska, K., Sionkowska, A., Ferreira-Da-Silva, F., Ferraz, M.P. and Monteiro, F.J. 2017. Phase behaviour and miscibility studies of collagen/silk fibroin macromolecular system in dilute solutions and solid state. Molecules 22.

Ghassemi, T., Shahroodi, A., Ebrahimzadeh, M.H., Mousavian, A., Movaffagh, J. and Moradi, A. 2018. Current Concepts in Scaffolding for Bone Tissue Engineering. Arch. bone Jt. Surg. 6: 90–99.

Gittens, R.A., Scheideler, L., Rupp, F., Hyzy, S.L., Geis-gerstorfer, J., Schwartz, Z. and Boyan, B.D. 2014. Acta Biomaterialia A review on the wettability of dental implant surfaces II: Biological and clinical aspects. Acta Biomater. 10: 2907–2918.

Gong, Y., Zhu, Y., Liu, Y., Ma, Z., Gao, C. and Shen, J. 2007. Layer-by-layer assembly of chondroitin sulfate and collagen on aminolyzed poly(l-lactic acid) porous scaffolds to enhance their chondrogenesis. Acta Biomater. 3: 677–685.

Gordon, M.K. and Hahn, R.A. 2010. Collagens. Cell Tissue Res. 339: 247–257.

Gorin, D.A., Yashchenok, A.M., Manturov, A.O., Kolesnikova, T.A. and Mohwald, H. 2009. Effect of Layer-by-Layer Electrostatic Assemblies on the Surface Potential and Current Voltage Characteristic of Metal - Insulator - Semiconductor Structures. Langmuir Artic. 25: 12529–12534.

Hodak, J., Etchenique, R., Calvo, E.J., Singhal, K. and Bartlett, P.N. 1997. Layer-by-Layer Self-Assembly of Glucose Oxidase with a Poly(allylamine)ferrocene Redox Mediator. Langmuir. 13: 2708–2716.

Huang, R., Li, W., Lv, X., Lei, Z., Bian, Y., Deng, H., Wang, H., Li, J. and Li, X. 2015. Biomimetic LBL structured nanofibrous matrices assembled by chitosan/collagen for promoting wound healing. Biomaterials. 53: 58–75.

Iler, R.K. 1966. Multilayers of Colloidal Particles. J. Colloid Interface Sci. 594: 569–594.

Im, D.S., Kim, M.H., Yoon, Y. Il and Park, W.H. 2016. Gelation behaviors and mechanism of silk fibroin according to the addition of nitrate salts. Int. J. Mol. Sci. 17: 1–9.

Inoue, S., Magoshi, J.U.N., Tanaka, T., Magoshi, Y. and Becker, M. 2000. Atomic Force Microscopy : Bombyx mori Silk Fibroin. J. Polym. Sci. Part B Polym. Phys. 38: 1436–1439.

Jana, S., Das, S., Gangopadhyay, U., Mondal, A. and Ghosh, P. 2013. A clue to understand environmental influence on friction and wear of diamond-like nanocomposite thin film. Adv. Tribol. 2013: 1-7.

Jang, S., Joo, B.S., Kim, S., Kong, K.J., Chang, H., Yu, B.D. and Han, M. 2015. Effects of proton irradiation on Si-nanocrystal/SiO multilayers: Study of photoluminescence and first-principles calculations. J. Mater. Chem. C. 3: 8574–8581.

Ji, H. 2010. Lysis of cultured cells for immunoprecipitation. Cold Spring Harb. Protoc. 5: 1–5.

Jung, D., Lee, K.H., Kwon, Y., Seo, J.H., Choi, B.-H., Yang, Y.J. and Cha, H.J. 2014. Multifunctional Adhesive Silk Fibroin with Blending of RGD-Bioconjugated Mussel Adhesive Protein. Biomacromolecules. 15: 1390–1398.

Kadler, K.E., Holmes, D.F., Trotter, J.A. and Chapman, J.A. 1996. Review Artice: Collagen fibril formation Karl. Biochem. J. 11: 1–11.

Kate, M.A., Palaskar, S. and Kapoor, P. 2017. Implant failure: A dentist' s nightmare. J. Dent. Implant. 6: 51–56.

Keeney, M, Jiang, X.Y., Yamane, M., Lee, M., Goodman, S. and Yang, F. 2015. Nanocoating for biomolecule delivery using layer-by-layer self-assembly. J. Mater. Chem. B. 3: 8757–8770.

Kern, W. 2006. The Evolution of Silicon Wafer Cleaning Technology. J. Electrochem. Soc. 137: 1887.

Kessler, J., Kapitán, J. and Bouř, P. 2015. First-Principles Predictions of Vibrational Raman Optical Activity of Globular Proteins. J. Phys. Chem. Lett. 6: 3314–3319.

Kim, J., Dhakal, K.P., Neupane, G.P., Guthold, M., Joseph, V.S., Hong, J.-D. and Lee, H. 2013. Simple method of DNA stretching on glass substrate for fluorescence image and spectroscopy. Nano-Bio Sensing, Imaging, Spectrosc. 19: 1-6.

Kim, K.H., Jeong, L., Park, H.N., Shin, S.Y., Park, W.H., Lee, S.C., Kim, T. Il, Park, Y.J., Seol, Y.J., Lee, Y.M., Ku, Y., Rhyu, I.C., Han, S.B. and Chung, C.P. 2005. Biological efficacy of silk fibroin nanofiber membranes for guided bone regeneration. J. Biotechnol. 120: 327–339.

Kim, S.H., Turnbull, J. and Guimond, S. 2011. Extracellular matrix and cell signalling: The dynamic cooperation of integrin, proteoglycan and growth factor receptor. J. Endocrinol. 209: 139–151.

Kittiphattanabawon, P., Benjakul, S., Visessanguan, W. and Shahidi, F. 2010. Isolation and characterization of collagen from the cartilages of brownbanded bamboo shark (Chiloscyllium punctatum) and blacktip shark (Carcharhinus limbatus). LWT - Food Sci. Technol. 43: 792–800.

Kubiak, K.J., Wilson, M.C.T., Mathia, T.G. and Carval, P. 2011. Wettability versus roughness of engineering surfaces. Wear. 271: 523–528.

Kumar, G. and Prabhu, K.N. 2007. Review of non-reactive and reactive wetting of liquids on surfaces. Adv. Colloid Interface Sci. 133: 61–89.

Lawande, S.A. and Lawande, G.S. 2016. Surface Modification of Titanium Endosseous Dental Implants and its Influence on Osseointegration: An Overview. Br. Biomed. Bull. 1–11.

Le Guéhennec, L., Soueidan, A., Layrolle, P. and Amouriq, Y. 2007. Surface treatments of titanium dental implants for rapid osseointegration. Dent. Mater. 23: 844–854.

Lee, C.H., Singla, A. and Lee, Y. 2001. Biomedical applications of collagen. Int. J. Pharm. 221: 1–22.

Li, L.-J., Kim, S.-N. and Cho, S.-A. 2016. Comparison of alkaline phosphatase activity of MC3T3-E1 cells cultured on different Ti surfaces: modified sandblasted with large grit and acid-etched (MSLA), laser-treated, and laser and acid-treated Ti surfaces. J. Adv. Prosthodont. 8: 235.

Li, Z.H., Ji, S.C., Wang, Y.Z., Shen, X.C. and Liang, H. 2013. Silk fibroin-based scaffolds for tissue engineering. Front. Mater. Sci. 7: 237–247.

Liu, X. and Zhang, K.Q. 2014. Silk Fiber - Molecular Formation Mechanism, Structure Property Relationship and Advanced Applications. Oligomerization Chem. Biol. Compd. 2: 69–102.

Ma, D., Wang, Y. and Dai, W. 2018. Silk fibroin-based biomaterials for musculoskeletal tissue engineering. Mater. Sci. Eng. C. 89: 456–469.

Ma, T., Ge, X., Zhang, Y. and Lin, Y. 2016. Effect of Titanium Surface Modifi cations of Dental Implants on Rapid Osseointegration. Interface Oral Heal. Sci. 247–256.

Majd, S.E., Kuijer, R., Köwitsch, A., Groth, T., Schmidt, T.A. and Sharma, P.K. 2014. Both hyaluronan and collagen type II keep proteoglycan 4 (lubricin) at the cartilage surface in a condition that provides low friction during boundary lubrication. Langmuir. 30: 14566–14572.

Mallick, K.K. and Winnett, J. 2014. 3D bioceramic foams for bone tissue engineering, Bone Substitute Biomaterials. Woodhead Publishing Limited. 118-141.

Mazur, M., Song, S., Domaradzki, J., Kaczmarek, D., Wojcieszak, D., Sieradzka, K., Placido, F. and Gemmellaro, P. 2011. Analysis of substrate type and thickness influence on wettability of Nb_2O_5 thin films. 2011 Int. Students Young Sci. Work. Photonics Microsystems. 94–98.

Meng, H.W., Chien, E.Y. and Chien, H.H. 2016. Dental implant bioactive surface modifications and their effects on osseointegration: a review. Biomark. Res. 4: 24.

Michel, M., Izquierdo, A., Decher, G., Voegel, J.C., Schaaf, P. and Ball, V. 2005. Layer by layer self-assembled polyelectrolyte multilayers with embedded phospholipid vesicles obtained by spraying: Integrity of the vesicles. Langmuir. 21: 7854–7859.

Michel, M., Toniazzo, V., Ruch, D. and Ball, V. 2012. Deposition Mechanisms in Layer-by-Layer or Step-by-Step Deposition Methods: From Elastic and Impermeable Films to Soft Membranes with Ion Exchange Properties. ISRN Mater. Sci. 2012: 1–13.

Mozafari, M., Ramedani, A., Zhang, Y.N., Mills, D.K. and States, U. 2016. Thin films for tissue engineering applications. Thin Film Coatings Biomater. Biomed. Appl. 167–195.

Muiznieks, L.D. and Keeley, F.W. 2013. Molecular assembly and mechanical properties of the extracellular matrix: A fibrous protein perspective. Biochim. Biophys. Acta-Mol. Basis Dis. 1832: 866–875.

Nawae, S., Meesane, J., Muensit, N. and Daengngam C. 2018. Layer-by-layer self-assembled films of silk fibroin/collagen/poly(diallyldimethylammonium chloride) as nucleating surface for osseointegration to design coated dental implant materials. Materials and Design. 160: 1158–1167.

Nijhawan, S., Bali, P. and Gupta, V. 2010. An Overview of the Effect of Topographic Surface Modifications of Endosteal Implants on Bone Performance and Bone Implant Responses. Int. J. Oral. 1: 77–82.

Nikolopoulou, F. and Tzortzopoulou, E. 2007. Salivary pH in Edentulous Patients Before and After Wearing Conventional Dentures and Implant Overdentures: A Clinical Study. Implant Dent. 16: 397–403.

Novales Jr., A.B., de Souza, S.L.S., de Barros, R.R.M., Pereira, K.K.Y., Iezzi, G. and Piattelli, A. 2010. In fluence of Implant Surfaces on Osseointegration. Braz. Dent. J. 21: 11.

Osipov, A., Osipova, L. and Zainullina, R. 2015. Raman Spectroscopy and Statistical Analysis of the Silicate Species and Group Connectivity in Cesium Silicate Glass Forming System. Int. J. Spectrosc. 2015: 1–15.

Owens, D.K. and Wendt, R.C. 1969. Estimation of the surface free energy of polymers. J. Appl. Polym. Sci. 13: 1741–1747.

Owens, G.J., Singh, R.K., Foroutan, F., Alqaysi, M., Han, C., Mahapatra, C. and Kim, H. 2016. Progress in Materials Science Sol-gel based materials for biomedical applications. Prog. Mater. Sci. J. 77: 1–79.

Parenteau-Bareil, R., Gauvin, R. and Berthod, F. 2010. Collagen-based biomaterials for tissue engineering applications. Materials (Basel). 3: 1863–1887.

Pavel, M., Renna, M., Park, S.J., Menzies, F.M., Ricketts, T., Füllgrabe, J., Ashkenazi, A., Frake, R.A., Lombarte, A.C., Bento, C.F., Franze, K. and Rubinsztein, D.C. 2018. Contact inhibition controls cell survival and proliferation via YAP/TAZ-autophagy axis. Nat. Commun. 9: 1–18.

Pellegrino, G., Tarsitano, A., Ferri, A., Corinaldesi, G., Bianchi, A. and Marchetti, C. 2018. Long-term results of osseointegrated implant-based dental rehabilitation in oncology patients reconstructed with a fibula free flap. Clin Implant Dent Relat Res. 2018: 1–8.

Phooplub. K. 2018. Development of low-dimensional materials in energy scavenging. Unpublished doctoral dissertation. Prince of Songkla University. 58.

Phooplub, K., Meesane, J. and Muensit, N. 2018. Development of Young's Modulus for Collagen Thin Films Reinforced with ZnO Nanorods Probed by Atomic Force Microscopy. Biomed. Phys. Eng. Express 4: 0–12.

Pieles, U., Bühler, T., Rechenberg, B. Von, Voelter, K., Snetivy, D. and Schlottig, F. 2007. Investigation of a unique nanostructured dental implant surface Investigation of a unique nanostructured dental implant surface. Eur. Cells Mater. 14: 95.

Qi, Y., Wang, H., Wei, K., Yang, Y., Zheng, R., Kim, I.S. and Zhang, K. 2017. A Review of Structure Construction of Silk Fibroin Biomaterials from Single Structures to Multi-Level Structures. Int. J. Mol. Sci. 18: 1-21.

Ramazanoglu, M. and Oshida, Y. 2011. Osseointegration and Bioscience of Implant Surfaces - Current Concepts at Bone-Implant Interface. Intech open. 57–82.

Richardson, J.J., Björnmalm, M. and Caruso, F. 2015. Technology-driven layer-by-layer assembly of nanofilms. Science. 348: 411–423.

Rising, A., Nimmervoll, H., Grip, S., Fernandez-Arias, A., Storckenfeldt, E., Knight, D.P., Vollrath, F. and Engström, W. 2005. Spider silk proteins-mechanical property and gene sequence. Zoolog. Sci. 22: 273–81.

Roa, J.J., Oncins, G., Diaz, J., Sanz, F. and Segarra, M. 2011. Calculation of Young's modulus value by means of AFM. Recent Pat. Nanotechnol. 5: 27–36.

Rockwood, D.D.N., Preda, R.R.C., Yücel, T., Wang, X., Lovett, M.L. and Kaplan, D.L. 2011. Materials fabrication from Bombyx mori silk fibroin. Nat. Protoc. 6: 1–43.

Rockwood, D.N., Preda, R.C., Yücel, T., Wang, X., Lovett, M.L. and Kaplan, D.L. 2013. Materials Fabrication from Bombyx mori Silk Fibroin. NIH Public Access 6: 220–231.

Rosa, A.L. and Beloti, M.M., 2003. Effect of cpTi surface roughness on human bone marrow cell attachment, proliferation, and differentiation. Braz. Dent. J. 14: 16–21.

Sahithi, B., Ansari, S., Hameeda, S., Sahithya, G., Durga Prasad, M. and Yogitha, L. 2013. A review on collagen based drug delivery systems. Indian J. Res. Pharm. Biotechnol. 1: 461–468.

Sammartino, G., Ehrenfest, D.M.D., Shibli, J.A. and Galindo-moreno, P. 2016. Tissue Engineering and Dental Implantology : Biomaterials , New Technologies , and Stem Cells. Biomed Res. Int. 2016: 1–3.

Sanches, L.M., Petri, D.F.S., Melo Carrasco, L.D. and Carmona-Ribeiro, A.M. 2015. The antimicrobial activity of free and immobilized poly (diallyldimethylammonium) chloride in nanoparticles of poly (methylmethacrylate). J. Nanobiotechnology. 13: 1–13.

Sánchez-Herencia, A.J. 2014. Water Based Colloidal Processing of Ceramic Laminates Water Based Colloidal Processing of Ceramic Laminates. Key Eng. Mater. 333: 39–48.

Shi, Q., Qian, Z., Liu, D. and Liu, H. 2017. Surface Modification of Dental Titanium Implant by Layer-by-Layer Electrostatic Self-Assembly. Front. Physiol. 8: 1–7.

Sinani, V.A., Koktysh, D.S., Yun, B.G., Matts, R.L., Pappas, T.C., Motamedi, M., Thomas, S.N. and Kotov, N.A. 2003. Collagen coating promotes biocompatibility of semiconductor nanoparticles in stratified LBL films. Nano Lett. 3: 1177–1182.

Smeets, R., Stadlinger, B., Schwarz, F., Beck-broichsitter, B., Jung, O., Precht, C., Kloss, F., Gröbe, A., Heiland, M. and Ebker, T. 2016. Impact of Dental Implant Surface Modifications on Osseointegration. Biomed Res. Int. 2016: 1-16.

Solá-Ruiz, M.-F., Pérez-martínez, C., Martín-del-Llano, J.-J., Carda-Batalla, C. and Labaig-Rueda, C. 2015. In vitro preliminary study of osteoblast response to surface roughness of titanium discs and topical application of melatonin. Med Oral Patol Oral Cir Bucal. 20: 88–93.

Song, W.-K., Liu, D., Sun, L.-L., Li, B.-F. and Hou, H. 2019. Physicochemical and Biocompatibility Properties of Type I Collagen from the Skin of Nile Tilapia (Oreochromis Niloticus) for Biomedical Applications. Mar. Drugs. 17: 137.

Sultana, S., Matsui, J., Mitsuishi, M. and Miyashita, T. 2008. Thickness Dependence of Surface Wettability Change by Photoreactive Polymer Nanosheets. Polym. J. 40: 953–957.

Sun, K., Li, H., Li, R., Nian, Z., Li, D. and Xu, C. 2014. Silk fibroin/collagen and silk fibroin/chitosan blended three-dimensional scaffolds for tissue engineering. Eur. J. Orthop. Surg. Traumatol. 25: 243–249.

Susana, G.-P., José Alejandro, H.-G., Luca, C., Hadi, H., Claudio, C., Alice, S., Roberto, C., Ilker, S.B., Athanassia, A. and Elisa, M. 2016. Low-cost and effective fabrication of biocompatible nanofibers from silk and cellulose-rich materials Low-cost and effective fabrication of biocompatible nanofibers from silk and cellulose-rich materials. ACS Biomater. Sci. Eng. 2: 526–534.

Talari, A.C.S., Movasaghi, Z., Rehman, S. and Rehman, I.U. 2015. Raman spectroscopy of biological tissues. Appl. Spectrosc. Rev. 50: 46–111.

Taniguchi, M., Pieracci, J.P. and Belfort, G. 2001. Effect of undulations on surface energy: A quantitative assessment. Langmuir. 17: 4312–4315.

Taraballi, F., Zanini, S., Lupo, C., Panseri, S., Cunha, C., Riccardi, C., Marcacci, M., Campione, M. and Cipolla, L. 2013. Amino and carboxyl plasma functionalization of collagen films for tissue engineering applications. J. Colloid Interface Sci. 394: 590–597.

Taubenberger, A. V., Woodruff, M.A., Bai, H., Muller, D.J. and Hutmacher, D.W. 2010. The effect of unlocking RGD-motifs in collagen I on pre-osteoblast adhesion and differentiation. Biomaterials. 31: 2827–2835.

Téllez S, C.A. 2017. Confocal Raman Spectroscopic Analysis of the Changes in Type I Collagen Resulting from Amide I Glycation. Biomed. J. Sci. Tech. Res. 1: 1–5.

Thomas, Y. 1805. An Essay on the Cohesion of Fluids. Phil Trans R Soc. 95: 65–87.

Ting, M., Jefferies, S.R., Xia, W., Engqvist, H. and Suzuki, J.B. 2017. Journal of Oral Implantology Classification and effects of implant surface modification on the bone : Human cell- based in-vitro studies. J. Oral Implantol. 43: 58–83.

Ude, A.U., Eshkoor, R.A., Zulkifili, R., Ariffin, A.K., Dzuraidah, A.W. and Azhari, C.H. 2014. Bombyx mori silk fibre and its composite: A review of contemporary developments. J. Mater. 57: 298–305.

Ueda, M. 2011. Tissue engineered bone: Application for implant surgery. Inflamm. Regen. 31: 202–218.

Vesentini, S., Redaelli, A. and Gautieri, A. 2013. Nanomechanics of collagen microfibrils. Muscles. Ligaments Tendons J. 3: 23–34.

Vootla, N.R. and Reddy, K.V. 2017. Osseointegration- Key Factors Affecting Its Success-An Overview. IOSR J. Dent. Med. Sci. 16: 62–68.

Walker, C., Mojares, E. and del Río Hernández, A. 2018. Role of Extracellular Matrix in Development and Cancer Progression, International Journal of Molecular Sciences. 19: 1-31.

Wang, G., Su, W., Chen, P. and Huang, T. 2017. Divalent Metal Ions Induced Osteogenic Differentiation of MC3T3E1. IOP Conf. Ser. Mater. Sci. Eng. 275: 1–8.

Wang, W., Caetano, G., Ambler, W.S., Blaker, J.J., Frade, M.A., Mandal, P., Diver, C. and Bartolo, P. 2016. Enhancing the hydrophilicity and cell attachment of 3D printed PCL/graphene scaffolds for bone tissue engineering. Materials. 9: 1-11.

Wu, T., Yu, S., Chen, D. and Wang, Y. 2017. Bionic design, materials and performance of bone tissue scaffolds. Materials. 10: 1-14.

Xiao, F.-X., Pagliaro, M., Xu, Y.-J. and Liu, B. 2016. Layer-by-layer assembly of versatile nanoarchitectures with diverse dimensionality: a new perspective for rational construction of multilayer assemblies. Chem. Soc. Rev. 45: 3088–3121.

Yamada, S., Yamamoto, K., Ikeda, T., Yanagiguchi, K. and Hayashi, Y. 2014. Potency of fish collagen as a scaffold for regenerative medicine. Biomed Res. Int. 2014: 2-8.

Yamamura, K., Miura, T., Kou, I., Muramatsu, T., Furusawa, M. and Yoshinari, M. 2015. Influence of various superhydrophilic treatments of titanium on the initial attachment, proliferation, and differentiation of osteoblast-like cells. Dent. Mater. J. 34: 120–127.

Yang, Y., Oh, N., Liu, Y., Chen, W., Oh, S., Appleford, M., Kim, S., Kim, K., Park, S. and Bumgardner, J. 2006. Enhancing Osseointegration Using Surface-Modified Titanium Implants. J. Miner. Met. Mater. Soc. 71–76.

Yarce, C., Pineda, D., Correa, C. and Salamanca, C. 2016. Relationship between Surface Properties and In Vitro Drug Release from a Compressed Matrix Containing an Amphiphilic Polymer Material. Pharmaceuticals. 9: 34.

Yusoff, I.I., Rohani, R. and Mohammad, A.W. 2018. Pressure driven conducting polymer membranes derived from layer by layer formation and characterization : A review. J. Eng. Sci. Technol. 11: 1183–1206.

Zafar, M.S. and Al-Samadani, K.H. 2014. Potential use of natural silk for bio-dental applications. J. Taibah Univ. Med. Sci. 9: 171–177.

Zareidoost, A., Yousefpour, M., Ghaseme, B. and Amanzadeh, A. 2013. The relationship of surface roughness and cell response of chemical surface modification of titanium. J. Mater. Sci. Mater. Med. 23: 1479–1488.

Zhang, L., Chen, H., Sun, J. and Shen, J. 2007. Layer-by-layer deposition of poly(diallyldimethylammonium chloride) and sodium silicate multilayers on silica-sphere-coated substrate-facile method to prepare a superhydrophobic surface. Chem. Mater. 19: 948–953.

Zhao, M.Y., Li, L.H., Li, B. and Zhou, C.R. 2014. LBL coating of type I collagen and hyaluronic acid on aminolyzed PLLA to enhance the cell-material interaction. Express Polym. Lett. 8: 322–335.

VITAE

Name Miss Safitree Nawae

Student ID 5610230017

Education Attainment

Degree	Name of Institution	Year of Graduation
Bachelor of Science (Physics)	Kasetsart University	2002
Master of Science (Physics)	Prince of Songkla University	2005

Scholarship Awards during Enrolment

1. Strategic Scholarships Fellowships Frontier Research Networks (Spectific for Southern region), The Office of the Higher Education Commission (OHEC), Thailand
2. Prince of Songkla University Graduate School Financial Support for Thesis Scholarships

List of publications and Proceedings

Nawae, S., Meesane, J., Muensit, N. and Daengngam C. 2018. Layer-by-layer self-assembled films of silk fibroin/collagen/poly(diallyldimethylammonium chloride) as nucleating surface for osseointegration to design coated dental implant materials. Materials and Design. 160: 1158–1167.